73215

Aphanitic Impact Melt Breccia
St. 3,1062 g

INTRODUCTION

73215 is a polymict breccia consisting largely of dark aphanitic impact melt and entrained clasts. It is characterized by structure indicating flow and shear during and after consolidation. Its composition is similar to other local aphanitic melt breccias in being a little higher in $A1_2O_3$ and a little lower in TiO_2 than the common low-K Fra Mauro basalt composition. Its melt appears to have crystallized close to 3.87 Ga ago. and the rock was exposed to radiation about 240 Ma ago.

73215 was collected from the landslide on the rim of the 10 m crater at Station 3. It is irregular in shape (Fig. 1), about 12 x 11 x 8.5 cm, and is blocky and tough. It has a few penetrative fractures. The rock is heterogeneous, with a light part that is pale yellow gray (5Y 8/1) and a dark part that is medium gray (N5). Flow gives the appearance of the light part, which occurs as lenses from 3 cm long down to minute veinlets, invading the dark part. The light part appears to be about 30% on the exterior, but the sawn interiors show rather less light material (Fig. 2). Most of the dark appears as closely packed aphanitic clasts embedded in a matrix of similar appearance, with subtle color variations. One surface is irregularly knobby, most of the others irregular, and one is a broken surface. There are many zap pits on two sides, fewer on the others, and none on the broken surface. No cavities are apparent. 73215 has been extensively studied in a consortium led by O. James. The sample was sawn to produce a slab in 1973, and most allocations were made from slab pieces. A second slab parallel to the first was cut in 1989 and subdivided for further studies (Fig. 3).

Figure 1: Pre-processing view of 73215, showing heterogeneous mix of light and dark banding. Cube and scale divisions are 1 cm. S-73-24270.

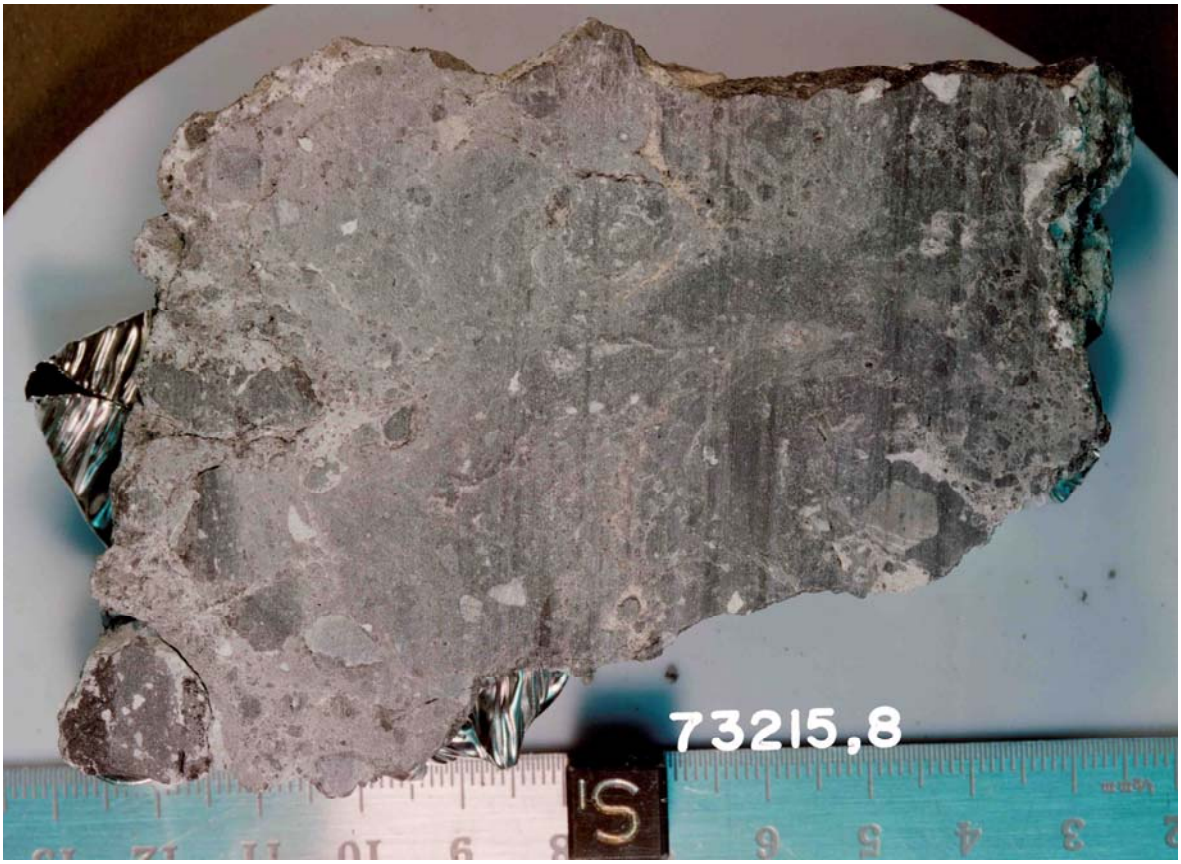

Figure 2: Sawn surface of end piece, 8, showing predominance of dark material and the apparent f low structures. Cube and scale divisions are 1 cm. S-76-26038.

PETROGRAPHY

The hand specimen is characterized by prominent structures, particularly now banding, formed by differential flow or shear or both during and after aggregation and consolidation (James et al. 1975 a,b). The bands are composed of several different kinds of gray to black aphanitic rock and different kinds of granulated clastic materials (Fig. 4). Locally, fault-like structures displace the banding. All types of aphanitic matrix consist of abundant small lithic and mineral fragments set in a dark groundmass (Fig. 5). The clasts are dominated by feldspathic impactites. (granulites) and other feldspathic lithologies. Felsites are minor, and clasts with basaltic textures are rare.

Simonds et al. (1974) listed 73215 as granular, with matrix feldspars and mafic minerals from 1 to 10 microns, and with about 50-60% feldspar. They found it to be one of the finest-grained of the micropoikilitic-subophitic-granular group, with the poorest development of tabular feldspar. They also noted the concentration of mineral clasts into vein-like segregations. Knoll and Stoffler (1976) classified 73215 as a dark, fine-grained, equigranular crystalline matrix breccia that partly contained areas of light-colored, coarser matrix, similar to 72215 and 72255. Dence et al. (1976) and Dence and Grieve (1976) described 73215 as genetically comparable with suevites, with the rock consisting of pods of dark breccia in a light porous clastic matrix. They noted the fine grain size of the dark material (1-2 microns in the finest areas) and the varied color. Shocked rounded plagioclases are conspicuous in it, and the clast population consists of highland rock types. However, there is not so much strongly shocked material as in terrestrial suevites. 73215 seems to be more thoroughly mixed than suevites, perhaps because of lower viscosity. They interpret the dark matrix to be shock melted material, with unshocked material from the upper 25 km of the crust and shocked materials from deeper levels; they infer that the melt is of Serenitatis origin.

By far the greater amount of work on 73215 has been done under the auspices of the James consortium (e.g. James et al., 1975 a,b; James and Blanchard, 1976). Consortium members also prefer a Serenitatis melt origin for the sample. James et al. (1976 a,b) identified a distinct groundmass that binds the fragments together. James (1976) clearly distinguished "matrix" as a binocular-microscope designation for aphanitic bulk masses distinct

Figure 3: End piece ,9 and new pieces sawn from it. Cube is 2.5 cm. S-8946188.

from separable clasts from "groundmass " as the fine-grained intergrowth that encloses even small clasts (Fig. 5b); that distinction will be followed here (this acceptance of the dark melt as matrix and the porous feldspathic materials as clasts is distinct from that of Dence et al., 1976, and Dence and Grieve, 1976, but is the status referred to by most workers). The dominant constituents of the groundmass are plagioclase and mafic minerals, with minor amounts of opaque oxides, and some Fe-metal and troilite. Generally felsic or silicic mesostasis is not apparent. The groundmass textures range from microintergranular to microsubophitic, and average grain size is from about 1 to 8 microns. The different aphanite types (color, coherency, etc.) relate to differences in groundmass grain-size and porosity, with the darkest aphanites being the least porous.

James et al. (1976 a,b) identified the enclosed fragments as dominated by plagioclases, with the lithic fragments mainly being coarse and fine granular feldspathic impactites. Many of these exist as monomict schlieren. The clasts have had diverse shock histories, with many showing no visible shock-induced microstructures. They have also had diverse thermal histories, with some, particularly felsites, being melted but most showing little if any thermal effects from breccia formation. Few reaction rims are visible, except for very unstable minerals such as silica and spinel; although overgrowth rims are present on some mafic clasts. In many matrix samples, elongate fragments show weak to strong parallel preferred orientations. Intensely sheared areas seen on sawed surfaces have higher porosity; shear and groundmass crystallization appear to have been contemporaneous.

James (1976 b ,c), James et al. (1976) and Nord and James (1977) made a detailed study of the aphanitic matrix]lithologies, which form the bulk of the rock. The rock formed as a mechanically mixed aggregate of crystalline clasts and silicate melt. The electron petrographic study of Nord and James (1977) confirms the melt origin of the groundmass, with microsubophitic laths of plagioclase clearly visible. While most of the aphanitic material is a matrix, similar material forms clast like bodies, most commonly gray spheroids within the matrix, and black clasts within granulated feldspathic materials. The gray spheroids at least are probably equivalent to cogenetic accretionary lapilli. The black aphanites form both angular particles and rinds and they are the darkest and toughest aphanites. James (1976) described several different types of aphanite

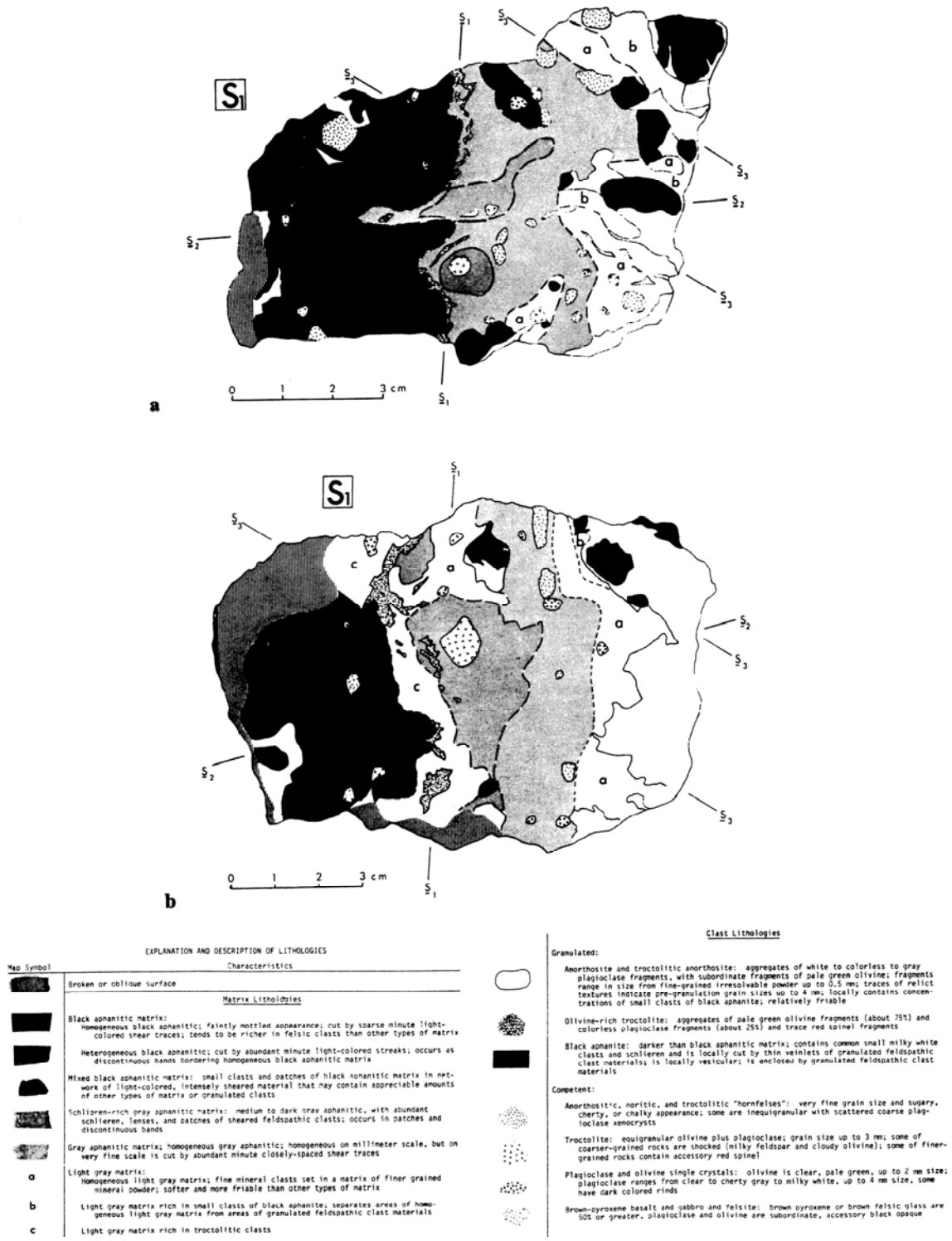

Figure 4: Maps of the Lithologies in sawed faces of 73215 as mapped by James (James et al., 1976a). a) is face of butt end,8 (as in Fig. 2). b) is one of the slab faces, parallel to but about 1.5 cm removed from a). James et al. (1975a).

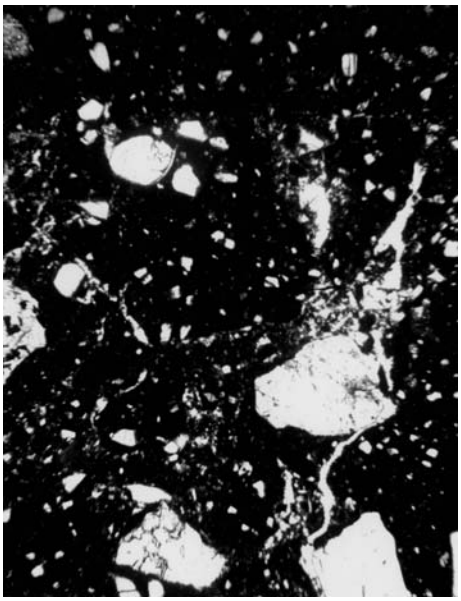

a

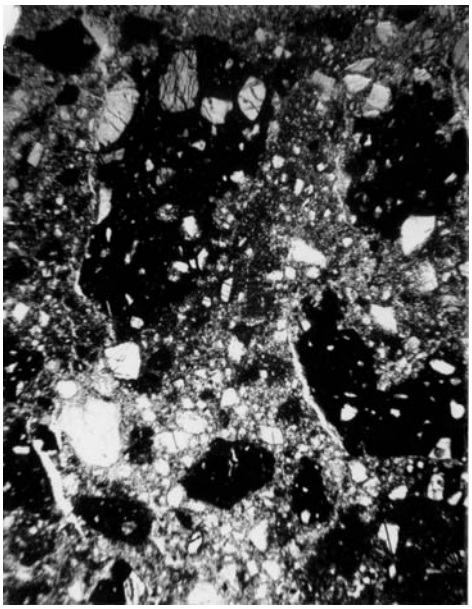

b

c

Figure 5: Photomicrographs of 73215,119. All plane transmitted light. a) general aphanitic matrix, with rounded and angular clasts, mainly plagioclases and feldspathic impactites. Field of view about 2 mm wide. b) mixed zone of aphanitic clasts and schlieren of porous feldspathic cataclasite with angular mineral fragments. Field of view about 2 mm. c) melt groundmass of the aphanite, showing distinction of fine-grained uniform melt from even small clasts. Field of view about 500 microns.

Table 1: Proportions of groundmass and clasts larger than 5 microns in various types of aphanite (vol. %). (James, 1976).

	Area counted (mm^2)	Clasts >5 μm			Groundmass
		Mafic minerals	Plagioclase	Lithic	
Gray aphanitic matrix (73215,245)	0.19	8.2	23.7	0	68.1
Black aphanitic matrix (73215,243)	0.21	5.1	20.5	3.3	71.1
Schlieren-rich gray aphanitic matrix (73215,103)	0.14	10.9	23.4	0	65.7
Gray aphanite spheroid ,38,57 (73215,350)	0.35	13.8	22.2	3.2	60.8
Black aphanite clast ,46,10 (73215,349)	0.35	7.9	23.4	0.1	68.8

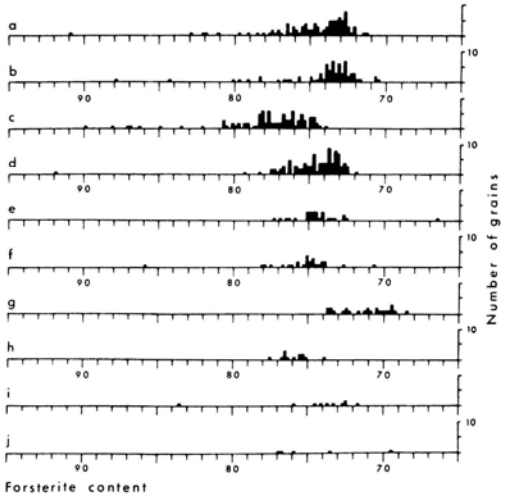

Olivine compositions in 73215 aphanites. Sizes of the areas surveyed are: ,228 matrix—1.9 mm^2; ,106 matrix—5 mm^2; ,228 clast-poor aphanite—0.41 mm^2; ,106 clast-poor aphanite—0.56 mm^2; ,46,10 black clast—1.3 mm^2; and ,38,57 gray spheroid—0.8 mm^2. (a) Clasts >25 μm in schlieren-rich gray matrix (,106). (b) Clasts >25 μm in gray matrix (,228). (c) Clasts >15 μm in gray spheroid ,38,57 (,350). (d) Clasts >15 μm in black clast ,46,10 (,349). (e) Clasts >10 μm in clast-poor aphanite in ,106. (f) Clasts >15 μm in clast-poor aphanite in ,228. (g) Groundmass grains and 5–25 μm clasts in gray matrix (,228), black matrix (,243) and schlieren-rich gray matrix (,103, ,106). (h) 5–25 μm clasts in gray spheroid ,38,57 (,350). (i) 5–25 μm clasts in black clast ,46,10 (,349). (j) Grains with euhedral outlines.

Figure 6: Compositions of olivines in 73215 aphanites. James (1976b)

(differing in color, grain-size, and mode of occurrence) providing modal data (Table 1) and mineral chemistry for both clasts and groundmass phases (Figs. 6-10). The aphanites contain from 60 to 70% groundmass melt, with the darkest aphanites having the most groundmass (Table 1).

In the groundmass the dominant minerals are plagioclase (An_{90-91}) and low-Ca pyroxene ($En_{74}Wo_3$), with minor olivine (Fo_{68-74}) (Figs. 6-9). The clasts were derived from a more homogeneous source than those in regolith breccias and most were cool and unshocked. Larger olivine clasts tend to be more magnesian than groundmass olivines. Pyroxene clasts too are more magnesian than groundmass pyroxenes. Most metal grains fall in the field appropriate for meteoritic metal. Most competent clasts were not deformed during or after breccia aggregation, although some devitrified maskelynites have outlines suggestive of plastic flow. Clasts of felsite show textures indicating plastic flow during incorporation. Other than felsites, few clasts show evidence of internal partial melting. A few clasts have overgrowth rims, and some mineral clasts much different from the groundmass have reacted or partly re-equilibrated, as described in detail in James (1976 b).

James (1976a,b) infers that the matrix aphanites were about 50% melt when it formed and the melt was fluid and superheated. During mixing with cold clasts in a debris cloud, the melt cooled and crystallized rapidly, producing lithologic banding as it flowed.

The most common clast-type is feldspathic impactite or granulite, commonly referred to as "anorthositic gabbro". Examples have been briefly described in the general consortium references; the most detailed descriptions are in James (1977 a), James and

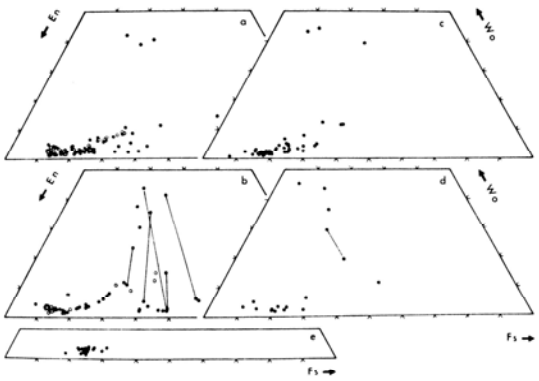

Wollastonite : enstatite : ferrosilite contents of pyroxenes in 73215 aphanites. Tie lines connect the compositions of pyroxenes co-existing in the same fragment, either as a patchy intergrowth of two phases or as host and exsolved lamellae. (a) Clasts in schlieren-rich gray matrix (,106). Filled circles are clasts >25 μm in matrix; open circles are clasts >10 μm in clast-poor aphanite. (b) Clasts in gray matrix (,228). Filled circles are clasts >25 μm in matrix; open circles are clasts >15 μm in clast-poor aphanite. (c) Clasts >15 μm in gray spheroid ,38,57 (,350). (d) Clasts >15 μm in black clast ,46,10 (,349). (e) Groundmass grains and 5–25 μm clasts in gray matrix (,228, ,245), black matrix (,243), schlieren-rich gray matrix (,103), and gray spheroid ,38,57 (,350).

Figure 7: Compositions of pyroxenes in 73215 aphanites. James (1976b).

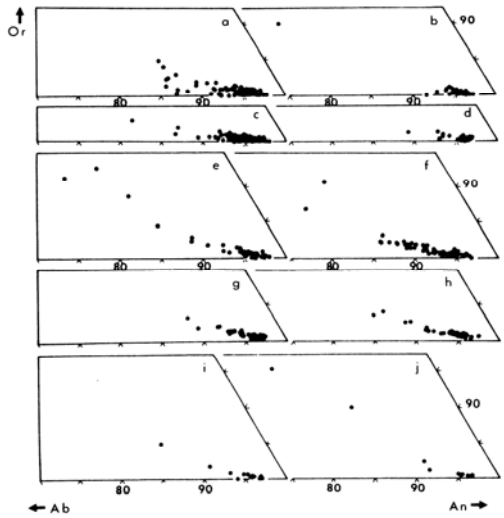

Orthoclase : albite : anorthite contents of feldspars in 73215 aphanites. (a) Clasts >25 μm in schlieren-rich gray matrix (,106). (b) Clasts >10 μm in clast-poor aphanite (,106). (c) Clasts > 25 μm in gray matrix (,228). (d) Clasts > 20 μm in clast-poor aphanite (,228). (e) 5–25 μm clasts and groundmass grains in gray matrix (,245) and schlieren-rich gray matrix (,103, ,106). (f) 5–25 μm clasts in black matrix (,243). (g) 5–25 μm clasts in black clast ,46,10 (,349). (h) 5–25 μm clasts in gray spheroid ,38,57 (,350). (i) Euhedral clasts in matrix aphanites. (j) Euhedral grains in zones surrounding clasts of felsic glass.

Figure 8: Compositions of plagioclases in 73215 aphanites. James (1976b).

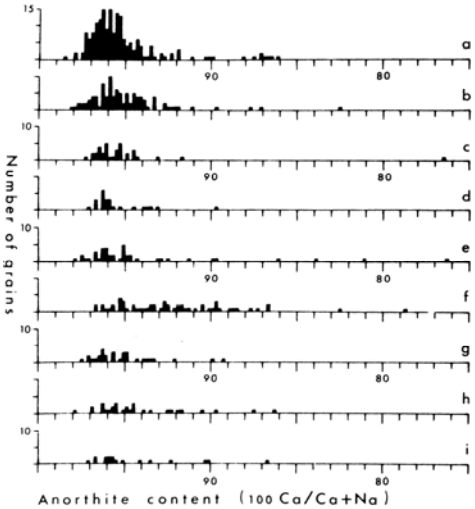

Plagioclase compositions in 73215 aphanites. (a) Clasts >25 μm in schlieren-rich gray matrix (,106). (b) Clasts >25 μm in gray matrix (,228). (c) Clasts >10 μm in clast-poor aphanite in ,106. (d) Clasts >20 μm in clast-poor aphanite in ,228. (e) Groundmass grains and 5–25 μm clasts in gray matrix (,245) and schlieren-rich gray matrix (,103, ,106). (f) 5-25 μm clasts in black matrix (,243). (g) 5–25 μm clasts in black clast ,46,10 (,349). (h) 5–25 μm clasts in gray spheroid ,38,57 (,350). (i) Euhedral clasts.

Figure 9: Compositions of plagioclases in 73215 aphanites. James (1976b).

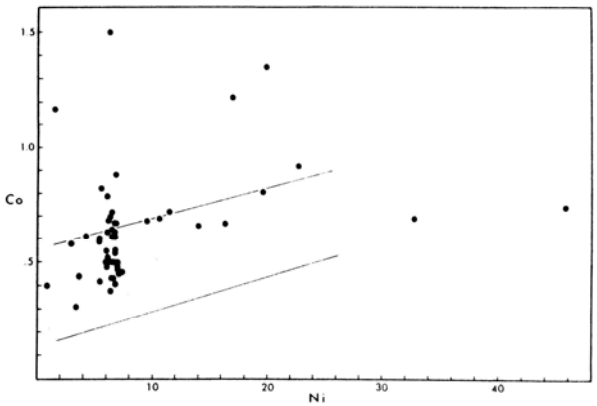

Compositions of metal particles in schlieren-rich gray matrix (,106). Particles analyzed were >10 μm across and were isolated within matrix; none were within clasts or had attached silicate mineral grains. The band passing through the diagram marks the range of compositions of meteoritic metal.

Figure 10: Compositions of metals in 73215 gray matrix James (1976b).

Hammarstrom (1977), and James and Hedenquist (1978). The three clasts described in detail by James and Hammarstrom (1977) and James (1977 a) were also analyzed by other members of the consortium. The clasts are modally anorthositic norites; one (29,9) is coarse poikilitic, the other two (45,25 and 45,33) are finer-grained and have mosaic as well as poikilitic textures. All are fairly well equilibrated, as shown by the microprobe analyses (Figs. 11-14), and are similar except that the coarser-grained sample has a lower mg' (Figs. 12,13). The cores of the large plagioclases, which are commonly surrounded by olivine "necklaces" are probably relics of pre-existing rocks. The impactites also contain trace constituents including K-feldspar, K-Si-rich glass, apatite, whitlockite, ilmenite, chromite, Ni-Fe metal, and baddeleyite. The metal compositions fall squarely in fields appropriate for meteorite contaminated rocks (Fig. 14). James and Hammarstrom interpret the texture and mineral chemical variations as being the products of crystallization from melts and solid-state crystallization. 29,9 is inferred to be mainly from melt, 45,25 mainly from solid-state crystallization, and 45,33 from melt (poikilitic) and solid-state (mosaic). Thus an origin as heated, partly-melted and/or recrystallized polymict breccias appears most likely. All three samples show healed fractures that post-date the recrystallization events.

James and Hedenquist (1978) described a 5 mm clast of spinel-bearing troctolitic basalt that consists of patches of basaltic-textured rock enclosed by very fine-grained granoblastic material (also analyzed by other members of the consortium). The boundaries between the two textures vary from sharp to gradational. The granoblastic material, a mosaic of anhedral grains, has grain sizes from 5 to 270 microns. The basaltic material has plagioclase laths 75-100 microns long with subhedral

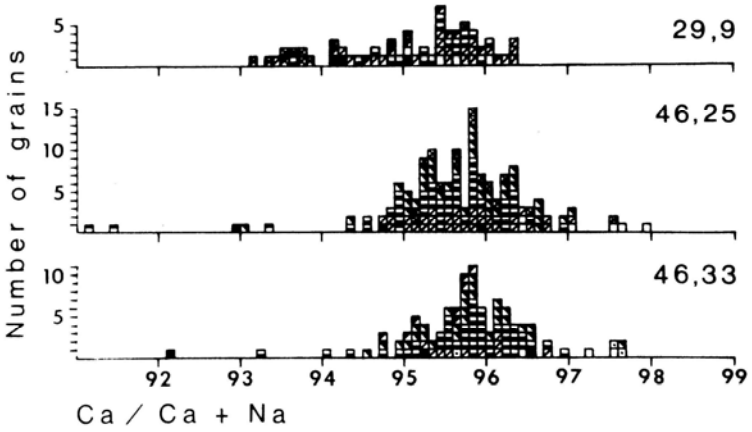

Histograms of Ca/Ca + Na contents in plagioclase in anorthositic gabbros. Textures and occurrences of the individual grains analyzed are indicated by the following symbols in the boxes on the diagrams: filled, cores containing K-feldspar inclusions; empty, inclusion-free cores and cores containing bubbles; small dot, cores containing glass inclusions; diagonal lines, rims on large grains; filled lower half, grains in oikocrysts; filled upper right corner, grains in mosaics; filled upper half, small euhedral grains in oikocrysts; filled upper left corner, globules included in olivine (29,9) or deformed, recovered plagioclase in mosaics (46,33); crosses, grains in lathy aggregate (46,25) or grain margins (29,9).

Figure 11: Compositions of plagioclases in feldspathic impactites in 73215. James and Hammarstrom (1977).

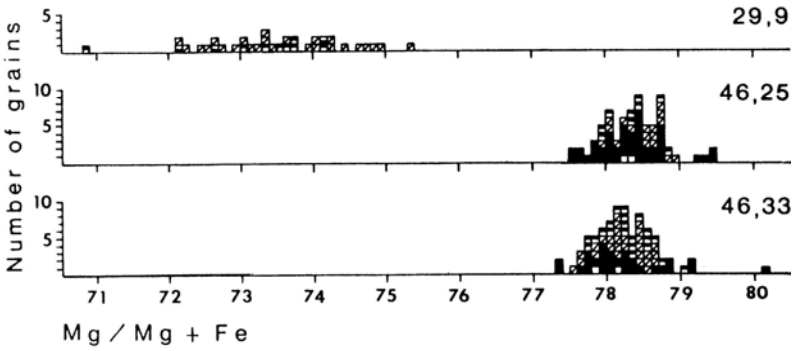

Histograms of Mg/Mg + Fe contents in olivines in anorthositic gabbros. Textures and occurrences of the individual grains analyzed are indicated by the following symbols in the boxes on the diagrams: filled, grains in mosaics; empty, centers of large grains; diagonal lines, globules forming "necklaces" in plagioclase grains; filled upper half, grains in oikocrysts; filled lower half, grain margins.

Figure 12: Compositions of olivines in feldspathic impactites in 73215. James and Hammarstrom (1977).

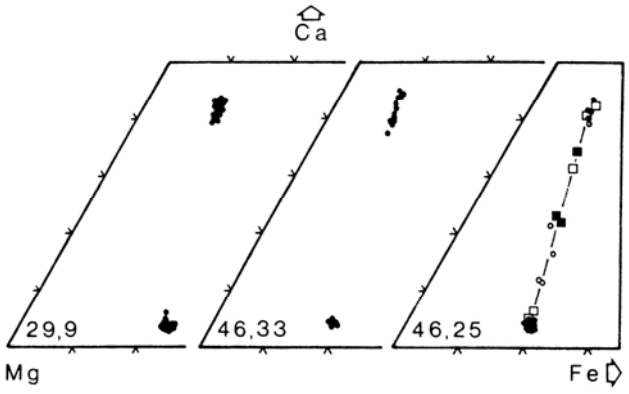

Ca:Mg:Fe of pyroxenes in anorthositic gabbros. Filled circles, grains forming oikocrysts. Open circles, analyses attempted of exsolution lamellae. Squares indicate analyses of pyroxene globules included in plagioclase grains in 46,25: open squares are individual phases in these globules; filled squares are expanded-beam analyses of the bulk globules.

Figure 13: Compositions of pyroxenes in feldspathic impactites in 73215. James and Hammarstrom (1977).

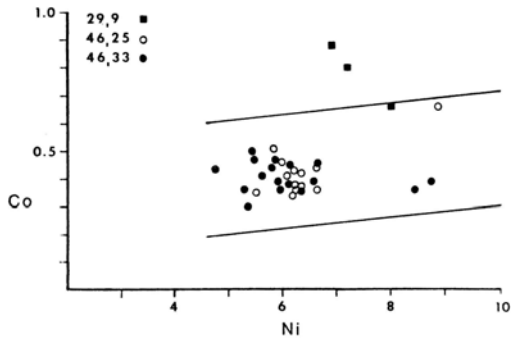

Ni–Co contents (wt.%) in metal grains in anorthositic gabbros. The area within the lines is the range of compositions of "meteoritic" metal (Goldstein and Yakowitz, 1971).

Figure 14: Compositions of metal grains in feldspathic bVactites in 73215. James and Hammarstrom (1977).

Olivine and pyroxene (50-200 microns) and pink spinel (20-50 microns). Both domains have the same mineral compositions (Fo_{87-82}, $En_{84}Wo_{4,}$ $En_{50}Wo_{44}$) except for plagioclase (basaltic An_{95-84}; granoblastic An_{99-90}). The troctolitic melt must have cooled quickly (otherwise the spinel would have been absorbed) and then partial granulation occurred. Subsequently the granulated areas were recrystallized. Several other clasts are like it

Nord and James (1977) made electron petrographic investigations of 200 micron clast of "hornfelsic norite". The clast had a grain size of 5 to 50 microns. The texture indicates that the clast was deformed and recrystallized prior to incorporation in the breccia. The transmission electron microscopy shows that recrystallization was extensive, producing straight contacts and triple junctions among small plagioclase grains. Antiphase domain boundaries are type (b) and probably formed by subsolidus recrystallization rather than from a phase transition during cooling. The orthopyroxenes have a moderate density of dislocations and a high density of linear defects (lamellae). The lamellae are clinopyroxene that are clinohypersthene, probably promoted by shock-induced shear. Hewins and Goldstein (1975a,b) analyzed metal in four clasts of "anorthositic hornfels" in 73215, fine-grained granoblastic materials. The metals are at the lower end of the meteoritic field. Two other clasts were analyzed: a devitrified shocked plagioclase has metal with high Co (2.29'0) but low Ni (M), and a light matrix breccia (presumably a porous feldspathic schlieren) has metal with low Ni (1-2%) but at the low end of the meteoritic field.

Neal et al. (1990d) reported preliminary data on a spinel troctolite assemblage in a clast in 73215, with olivine (Fo_{89-92}), Plagioclase (An_{91-96}) and Mg-Al spinel with 8-11 wt % Cr_2O_3. Individual grains are unzoned. Eckert et al. (1991 a,b,c) reported further on this class, which appears to be a statically recrystallized cumulate rock. The mode is about 78% plagioclase, 21 % olivine, 2% spinel, with minor high-Ca and low-Ca pyroxene, FeNi metal, and chromite (Eckert et al. 1991 a). The pyroxene may not be in equilibrium with the rest of the assemblage. The olivines have very low CaO abundances, indicative of slow cooling. The mineral assemblage appears to have originated at relatively high pressure, deeper than about 25 km. Eckert et al. (1991 b) also reported a cataclasized dunite clast, with spinel and a glass mesostasis cored by an SiO_2

phase. The main silicates have ranges in composition: olivine Fo_{72-92}, plagioclase An_{90-97}.

Hansen et al. (1979 b) and Smith et al. (1980) reported some precise minor element data (microprobe) for olivines and low-Ca pyroxenes in a feldspathic impactite and an Mg-rich plutonic troctolitic rock The reports are not very specific about the parent lithologies. The Mg-rich plutonic has olivine with Fa_{90-91} and plagioclase with An_{96}, while the feldspathic impactite is more iron-rich (Fo_{76}). Steele et al. (1980) reported ion probe data for plagioclase in the Mg-rich troctolite.

James and Hammarstrom (1976) and Nord and James (1977) gave a detailed description of a felsite class that was also studied by other members of the consortium. The felsite comprises two components: crystalline felsite and veins of silicic glass. James and Hammarstrom (1976) detail the textures and the mineral and glass chemistry (Figs. 15-17; Table 2), and their genetic inferences there from. The crystalline felsite consists mainly of a vermicular intergrowth of quartz (40%) and K-feldspar (60%); minor plagioclase forms blebs associated with the quartz. Trace amounts of ilmenite, zircon, olivine, apatite, and whitlockite are present, and some mosaic patches include pyroxene. Some of the feldspars have an unusual ternary composition (Fig. 15); the electron petrographic studies show this ternary feldspar to be a homogeneous phase, with some probable initial attempts at phase separation apparent (Nord and James, 1977). The minerals do not show shock effects; dislocation density in the quartz is very low, and that in the K-feldspar not much higher. The felsic glass is varied in vesicularity, color, and relict mineral content; second generation minerals quenched from the glass are present. Most of the glass is brown, with abundant needle-like crystallites. Electron petrographic study shows that the bulk of this

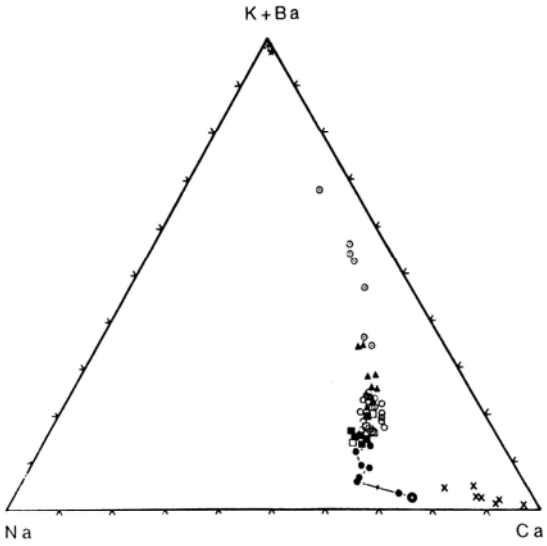

K + Ba : Na : Ca contents of feldspars in felsite clast. Large circle, average of 14 analyses in core of zoned plagioclase grain (Fig. 1d); small filled circles, traverse from inner to outer boundary of rim of zoned plagioclase grain (3 μm steps, arrow indicates direction of traverse). Filled squares, points in equant 0.2 mm plagioclase grain. Open squares, plagioclase grains in mosaics. Small open circles, plagioclase grains in vermicular intergrowth. Filled triangles, centers of plagioclase relics in felsic glass. Small dotted circles, reacted and second-generation inclusion-rich plagioclase in felsic glass. Asterisk, average of 26 analyses of K-feldspar in vermicular intergrowth. Filled star, average of 11 analyses of second-generation K-feldspar in felsic glass. ×, small plagioclase grains in mixed material at edge of clast.

Figure 15: Compositions of feldspars in the felsite clast in 73215. James and Hammarstrom, 1977.

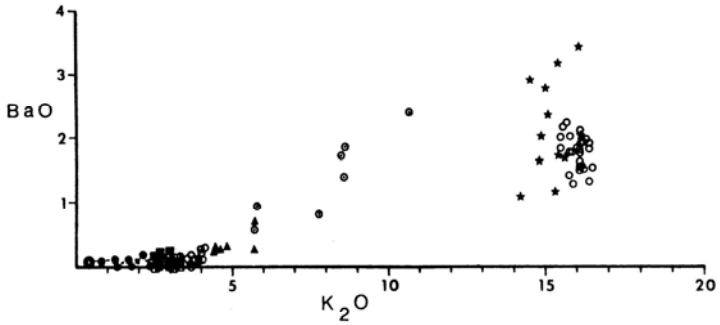

K_2O vs. BaO contents in feldspars in felsite clast. Symbols are as in Fig. 2, except: open circles indicate all analyses of plagioclase and K-feldspar in vermicular intergrowth; filled stars indicate all analyses of second-generation K-feldspar in felsic glass; plagioclase in mixed material is not shown.

Figure 16: Compositions of feldspars in the felsite clast in 73215. James and Hammarstrom, 1977.

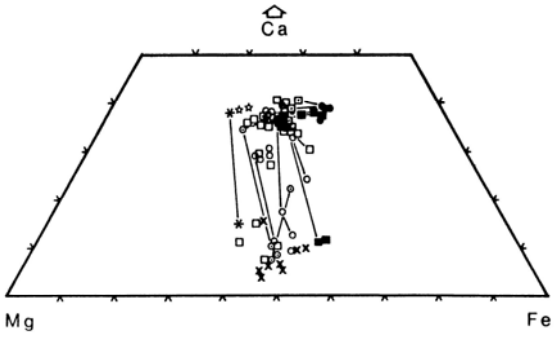

Ca:Mg:Fe contents of pyroxenes in felsite clast. Filled circles, centers of pyroxene grains in crystalline felsite. Filled squares, centers of pyroxene relics in felsic glass. Open symbols are second-generation pyroxenes, as follows: dotted squares, edges of grains in crystalline felsite or edges of relics in felsic glass; circles, rims on olivine relics; squares, prismatic crystals; dotted circles, large blocky grains with associated Fe metal and troilite; stars, rims on ilmenite relics; asterisks, rim on olivine relic at edge of clast. ×, grains in mixed material at edge of clast. Tie lines connect compositions of points in the same grains.

Figure 17: Compositions of pyroxenes in the felsite clast in 73215. James and Hammarstrom, 1977.

material is uncrystallized (Nord and James, 1977). All the glasses are Si- and K-rich. The crystalline felsite clearly crystallized from a melt to produce a texture similar to terrestrial granophyres. The felsic glass forms veins and patches and was emplaced as dikelets, not by in situ melting. The fracturing and diking preceded incorporation of the clast into the breccia. Nonetheless, the parent of the glass, presumably shock produced, must have been from the same felsite body. The bulk clast was quite hot when it was incorporated in the breccia, because some of the glass it contains did form at that time by in situ melting. It was then rapidly cooled, precipitating second generation pyroxene and K-feldspar.

Miura (1988) reported the presence of "anomalous" plagioclases (i.e., deficient in Al, Na) in 73215 as is present in some lunar basalts. However, the plagioclases are not otherwise described. Bickel and Warner (1978a) listed 73215,234 in their study of plutonic and granulitic lunar samples, but did not otherwise provide any data on such sample from 73215.

CHEMISTRY

Many chemical analyses have been made of bulk rock, aphanite samples, and clasts or schlieren. Both bulk rock/matrix and aphanite analyses are compiled in Table 3, with the rare earth elements plotted in Figure 18. Microprobe defocused beam analyses of the groundmass are reproduced as Table 4 and Figure 19. Clast analyses are compiled in Table 5, with the rare earth elements plotted in Figures 20 and 21. A guide to how some of the split numbers correspond with lithologies is shown in Figure 22 and Table 6 (from James and Blanchard, 1976). (The text of Bence et al. (1975) erroneously refers to 72315 where 73215 is intended.) Ehmann et al, (1975 a,b) reported an O analysis of 47.2% for ,172 aphanite. James et al. (1975a) reported that no CH4 or CD4 in excess of 0.06 ug/g were found in interior or exterior samples.

The matrix and bulk sample analyses are dominated by the aphanitic phase. In general both black and gray aphanites have the same composition; however, at least some of the black materials appear to be higher in volatile and incompatible elements. Individual differences are probably a result of variation in included clasts (e.g. James et al., 1975 a,b). All matrix and aphanite samples are aluminous, low-K Fra Mauro basalt compositions, distinguished from the typical Apollo 17 impact melt by the lower TiO_2 and higher $A1_2O_3$ of the 73215 materials. The incompatible elements show a range from about 70x chondrites to about 120 x chondrites, part or all of which is probably a reflection of varied clast contents (e.g., Blanchard et al., 1976) as well as the small sample sizes; similar considerations probably apply to variations in Co and Ni as well. The Zn is much lower than that found in typical soils or regolith breccia, lending weight to the argument that 73215 was not created from regolith, but from a larger event (James et al., 1975 a). The meteoritic siderophiles in the aphanites fall into Group 2 of Morgan et al.(1976), attributed to Serenitatis, and distinct from the Boulder 1, Station 2 aphanites. Although one analyzed (38,57) appeared to be a group 6 (Morgan et al., 1976) a second analysis appeared quite normal; the reason for the first analysis being different remains a mystery (Morgan and Petrie, 1979 a,b).

James (1976) made defocused beam microprobe analyses of the varied aphanites (with subtraction of clast compositions) to attempt to obtain the composition of the melt groundmass (Table 4). The groundmass composition is similar to that of the bulk aphanites and is fairly homogeneous.

Table 2: Compositions of minor phases and glasses in felsite (wt%; electron microprobe analyses).
(James and Hammarstrom, 1977).

	(1)	(2)	(3)	(4)	(5)	(6)	(7)	(8)	(9)
SiO_2	0.22	0.28	—	—	74.2	78.2	76.7	76.8	78.1
TiO_2	50.7	1.79	—	—	0.73	0.36	0.65	0.28	0.49
Al_2O_3	0.13	22.2	—	—	13.4	12.9	13.1	13.4	12.6
FeO	45.4	31.8	1.81	0.34	1.24	0.61	0.81	0.38	0.40
MgO	1.15	1.89	2.29	0.07	0.04	0.01	0.04	0.03	0.03
CaO	0.09	0.09	38.7	53.4	0.62	0.64	0.79	0.75	0.77
Na_2O	—	—	—	—	0.10	0.14	0.21	0.17	0.30
K_2O	—	—	—	—	9.58	6.90	7.20	7.88	7.21
BaO	—	—	—	—	0.26	0.06	0.04	0.11	0.10
MnO	0.47	0.51	—	—	0.02	0.02	0.02	0.01	<0.01
Cr_2O_3	0.38	38.1	—	—	0.03	0.01	0.02	0.01	0.02
Y_2O_3	—	—	4.48	0.37	—	—	—	—	—
La_2O_3	—	—	1.07	0.13	—	—	—	—	—
Ce_2O_3	—	—	3.01	0.23	—	—	—	—	—
Nd_2O_3	—	—	1.63	0.19	—	—	—	—	—
Sm_2O_3	—	—	0.59	0.06	—	—	—	—	—
Gd_2O_3	—	—	1.37	0.20	—	—	—	—	—
P_2O_5	—	—	40.5	40.4	0.21	0.04	0.26	0.09	0.20
ZrO_2	—	—	—	—	0.11	0.13	0.22	0.04	0.07
F	—	—	0.43	2.88	—	—	—	—	—
Cl	—	—	0.29	0.89	—	—	—	—	—
Total	98.54	96.66	96.17	99.16	100.54	100.02	100.06	99.95	100.29

(1) Ilmenite: average of 12 analyses of grains in felsic glass and crystalline felsite.

(2) Aluminous chromite: inclusion in ilmenite grain in crystalline felsite (low total due to small size of grain).

(3) Whitlockite: average of three analyses of grains in crystalline felsite (low total due to destruction of grains during analysis).

(4) Apatite: average of eight analyses of grains in felsic glass and crystalline felsite.

(5) Brown glass: average of 20 analyses.

(6) Uncrystallized colorless glass in felsic glass veins and patches: average of ten analyses.

(7) Uncrystallized colorless glass haloes around second-generation and relict mafic mineral grains: average of 12 analyses.

(8) Uncrystallized colorless glass selvages in vermicular intergrowth in crystalline felsite: average of five analyses.

(9) Uncrystallized colorless glass bands at contact of crystalline felsite and matrix: average of five analyses.

Table 3: Chemical analyses of bulk rockhnatrix and aphanites in 73215.

Split	,161	,161	,74	,184	,177	,186	,76	,170 ,9006	,? blckmx
wt%									
SiO_2	48.1		46.1	46.8	46.1	46.7			
TiO_2	0.8		1.1	0.4	1.1	0.6			
Al_2O_3	19.4		21.7	21.5	19.9	20.4			
Cr_2O_3	0.168		0.200	0.230	0.221	0.46			
FeO	7.64		7.39	7.20	7.28				
MnO	0.123		0.104	0.099	0.119				
MgO	10.2		10.2	11.8	11.1	11.0			
CaO	11.0		12.2	11.8	12.3	11.5			
Na_2O	0.624		0.495	0.488	0.487				
K_2O	0.656		0.167	0.170	0.191	0.31			
P_2O_5									
ppm									
Sc	14.3		14.4	13.5	14.1	23.7			
V									
Co	24.5		25.6	27.8	21.2	27.1			
Ni	200	152	150	190	150		163	118	
Rb	5.5	8.93			3.0	13.6	2.3	2.34	
Sr									
Y									
Zr									
Nb									
Hf	13.7		9.5	8.9	7.8	13.9			
Ba									
Th	7.5		3.7	4.2	3.6				4.332
U		2.2					1.2	1.1	1.207
Cs	0.18	0.56			0.123	0.57	0.164	0.107	
Ta	2.3		1.5	1.4	1.4				2.556
Pb									
La	41		25.5	25.6	24.3	36.1			
Ce	105		69	68	63	86			
Pr									
Nd	62				37.3	55			
Sm	18.6		11.9	12.2	10.7	16.8			
Eu	1.63		1.41	1.37	1.35	1.55			
Gd	20.6				13.0	15.0			
Tb	3.55		2.8	2.7	2.11	3.3			
Dy	23.5				14.6	20.0			
Ho									
Er									
Tm									
Yb	13.0		8.8	9.1	8.5	12.1			
Lu	1.91		1.2	1.35	1.1	1.84			
Li									
Be									
B									
C									
N									
S									
F									
Cl									
Br		0.106					0.026	0.0092	
Cu									
Zn	<5	2.5			2.5		2.0	1.9	
ppb									
Au		2.4					2.7	1.65	
Ir		4.3					4.9	3.49	
I									
At									
Ga	4160				5300	5300			
Ge		252					175	82	
As									
Se		72					72	39	
Mo									
Te									
Ru									
Rh									
Pd									
Ag		0.73					0.91	20	
Cd		12.4					18.4	1.3	
In									
Sn									
Sb		1.2					0.95	0.89	
Te		4.9					5.9		
W									
Re		0.34					0.37	0.274	
Os									
Pt									
Hg									
Tl		5.0					4.3	2.8	
Bi		0.28					0.52	0.75	
	(1)	(1,8,10)	(1)	(1)	(1)	(1)	(1,8,10)	(1,8,10)	(1) (a)

References and methods:
(1) James et al. (1975a); INAA, RNAA, AAS. (a) isotope dilution/mass spec.
(8) Higuchi and Morgan (1975a,b); RNAA]
(10) Morgan et al. (1976); RNAA

Table 3 continued: Chemical analyses of bulk rock/matrix and aphanites in 73215.

Split	,146	,139	,156	,273	Split
wt %	+ ,147				wt %
SiO_2					SiO_2
TiO_2					TiO_2
Al_2O_3					Al_2O_3
Cr_2O_3					Cr_2O_3
FeO					FeO
MnO					MnO
MgO					MgO
CaO					CaO
Na_2O					Na_2O
K_2O					K_2O
P_2O_5					P_2O_5
ppm					ppm
Sc					Sc
V					V
Co					Co
Ni					Ni
Rb					Rb
Sr					Sr
Y					Y
Zr					Zr
Nb					Nb
Hf					Hf
Ba					Ba
Th					Th
U					U
Cs					Cs
Ta					Ta
Pb					Pb
La					La
Ce					Ce
Pr					Pr
Nd					Nd
Sm					Sm
Eu					Eu
Gd					Gd
Tb					Tb
Dy					Dy
Ho					Ho
Er					Er
Tm					Tm
Yb					Yb
Lu					Lu
Li					Li
Be					Be
B					B
C	32	27	24	13	C
N	<1.5	<1.5	<1.5	<1.5	N
S	234	199	183	284	S
F					F
Cl					Cl
Br					Br
Cu					Cu
Zn					Zn
ppb					ppb
Au					Au
Ir					Ir
I					I
At					At
Ga					Ga
Ge					Ge
As					As
Se					Se
Mo					Mo
Tc					Tc
Ru					Ru
Rh					Rh
Pd					Pd
Ag					Ag
Cd					Cd
In					In
Sn					Sn
Sb					Sb
Te					Te
W					W
Re					Re
Os					Os
Pt					Pt
Hg					Hg
Tl					Tl
Bi					Bi
	(1)	(1)	(1)	(1)	

References and methods: James et al. (1975a); combustion/mass spectrometry

Table 3 continued: Chemical analyses of bulk rock/matrix and aphanites in 73215.

Split	,94	,49	,140	,32	,90	Avg. of 11	,81 black	,136 gray	Split
wt%									wt%
SiO_2	47.67	46.47	46.53	46.75	46.34	46.4			SiO_2
TiO_2	0.23	0.63	0.65	0.67	0.68	0.7			TiO_2
Al_2O_3	23.4	22.95	20.66	20.64	20.07	20.6			Al_2O_3
Cr_2O_3		0.118	0.204			0.25			Cr_2O_3
FeO	5.39	6.58	7.73	7.56	7.79	7.3			FeO
MnO						0.104			MnO
MgO	9.16	9.39	11.47	11.16	11.79	11.6			MgO
CaO	12.81	13.25	12.10	12.2	11.79	11.9			CaO
Na_2O	0.83	0.49	0.58	0.42	0.80	0.50			Na_2O
K_2O	0.19	0.23	0.20	0.20	0.31	0.20			K_2O
P_2O_5							0.33	0.21	P_2O_5
ppm									ppm
Sc		11	16			14.7			Sc
V		39	52						V
Co		19	24			25.3			Co
Ni		160	200			165			Ni
Rb	1.99	4.73	2.2	1.4	7.7				Rb
Sr									Sr
Y	87	58	93	85	127				Y
Zr	400	208	300	354	665				Zr
Nb	25.6	16.8	23.6	23.5	42				Nb
Hf	9.90	6.1	8.41	8.0	14.5	9.5			Hf
Ba	300	211	315	350	432				Ba
Th	4.81	3.49	4.51	4.20	7.3	4.1			Th
U	1.23	0.87	1.24	1.08	1.76		1	1.9	U
Cs									Cs
Ta						1.4			Ta
Pb	2.79	2.42	2.86	2.17	5.15				Pb
La	26	16.6	25	24.5	37.2	27.0			La
Ce	68	41	71	68	99.6	70			Ce
Pr	9.0	5.9	9.8	8.96	13.3				Pr
Nd	38	22.2	39.9	36.3	53				Nd
Sm	11.0	6.42	11.1	9.55	15.6	12.5			Sm
Eu	1.39	1.25	1.45	1.19	1.59	1.43			Eu
Gd	11.0	8.14	13.9	10.7	18.3				Gd
Tb	2.28	1.45	2.35	1.98	3.24	2.6			Tb
Dy	14.2	8.80	14.5	12.9	21.3				Dy
Ho	3.12	2.12	3.30	2.90	4.61				Ho
Er	9.30	6.20	9.80	8.60	13.9				Er
Tm	1.43	0.91	1.44	1.24	2.05				Tm
Yb	8.67	5.34	8.73	7.51	12.4	9.1			Yb
Lu	1.34	0.86	1.35	1.16	1.93	1.30			Lu
Li									Li
Be									Be
B									B
C									C
N									N
S									S
F								80	F
Cl							6.1(a)	36.1(a)	Cl
Br							53(a)	217(a)	Br
Cu									Cu
Zn									Zn
ppb									ppb
Au									Au
Ir									Ir
I							2.2		I
At									At
Ga									Ga
Ge									Ge
As									As
Se									Se
Mo									Mo
Tc									Tc
Ru									Ru
Rh									Rh
Pd									Pd
Ag									Ag
Cd									Cd
In									In
Sn									Sn
Sb									Sb
Te									Te
W									W
Re									Re
Os									Os
Pt									Pt
Hg									Hg
Tl									Tl
Bi									Bi
	(2)	(2)	(2)	(2)	(2)	(3)	(12)	(12)	

References and methods:
(2) Bence et al. (1975); EMP/spark source mass spectrometry
(3) Blanchard et al (1976); INAA
(12) Jovanovic and Reed (1976a,b, 1980a);neutron and photon activation analysis

Notes:
(a) combined leach and residue

Table 3 continued: Chemical analyses of bulk rock/matrix and aphanites in 73215.

Split	,46,2	,46,7	,46,10	,46,10.5	,46,19	,46,19.4	,38,17	,38,32	,38,57	,38,57.6	,38,57
wt%	a	a	a	a	a		b	b	b	b	b
SiO_2		46.7	45.6		46.3		46.7	46.4	45.9		
TiO_2		1.3	1.1		1.0		0.8	0.9	0.8		
Al_2O_3		19.0	19.8		20.0		21.8	20.3	20.7		
Cr_2O_3	0.24	0.28	0.25		0.25		0.23	0.23	0.21		
FeO	8.32	8.75	8.13		7.87		6.97	7.04	6.94		
MnO		0.121	0.106		0.111		0.089	0.108	0.093		
MgO		12.6	12.0		11.7		10.7	12.4	11.8		
CaO		11.1	11.5		11.7		12.3	11.6	11.4		
Na_2O	0.52	0.50	0.52		0.54		0.54	0.49	0.52		
K_2O		0.20	0.22		0.22		0.20	0.19	0.16		
P_2O_5											
ppm											
Sc	15.9	17.1	15.7		15.8		11.9	13.2	12.0		
V											
Co	22.7	33.6	36.0		24.9		26.6	26.7	30.0		
Ni	40.0	220	290	167	150	137	230	160	250	596	195
Rb				3.02		3.2				2.84	
Sr											
Y											
Zr											
Nb											
Hf	9.8	9.7	10.7		9.9		9.1	7.7	8.3		
Ba											
Th	4.0	4.3	4.6		4.4		4.1	4.3	3.9		
U				1.100		1.130				1.040	1.380
Cs				0.110		0.141				0.109	
Ta	2.3	1.5	1.2		1.4		1.5	1.3	1.4		
Pb											
La	26.6	28.8	27.7		27.5		25.9	32.0	23.4		
Ce	69	78	74		73		67	86	65		
Pr											
Nd											
Sm	12.1	13.5	12.2		12.4		11.5	14.9	10.2		
Eu	1.44	1.38	1.41		1.41		1.49	1.53	1.44		
Gd											
Tb	2.7	2.9	2.9		2.7		2.9	3.8	2.6		
Dy											
Ho											
Er											
Tm											
Yb	9.1	9.7	9.4		9.3		8.4	10.3	7.9		
Lu	1.21	1.35	1.27		1.27		1.21	1.40	1.09		
Li											
Be											
B											
C											
N											
S											
F											
Cl						0.023					
Br				0.0358						0.250	
Cu											
Zn				1.9		1.9				2.3	2.9
ppb											
Au				2.01		2.0				5.63	3.4
Ir				3.24		3.5				27.3	5.4
I											
At											
Ga											
Ge				135		216				315	320
As											
Se				57		110				59	73
Mo											
Tc											
Ru											
Rh											
Pd				8.4		5.9				31.5	11.6
Ag				0.72		0.7				5.91	0.98
Cd				5.4		7.4				5.4	5.0
In				11.4		1.8				59.8*	<6
Sn											
Sb				1.65						32.7	1.51
Te				7.2						8.7	
W											
Re				0.343		0.32				2.61	0.56
Os				3.56		3.1				34.1	6.3
Pt											
Hg											
Tl				1.7		2.5				2.1	2.7
Bi				0.59						0.62	0.46
	(3)	(3)	(3)	(9,10)	(3)	(10)	(3)	(3)	(3)	(9,10)	(11)

References and methods:
(3) Blanchard et al. (1976); INAA,AAS
(9) Gros et al. (1976); RNAA
(10) Morgan et al. (1976); RNAA
(11) Morgan and Petrie (1979a,b);RNAA

Notes:
*doubtful value according to authors
a black aphanite clasts
b gray aphanite spheroids

Table 3 continued: Chemical analyses of bulk rock/matrix and aphanites in 73215.

Split	,176	,66	,68	,160	,163	,166	,172(#)	,0	,52	,155	,158	,401
wt%	gray	gray	gray	black	black	black	gray					
SiO_2	48.8											
TiO_2												
Al_2O_3	21.4											
Cr_2O_3	0.250	0.200	0.206	0.210	0.191	0.200	0.234					
FeO	8.5	6.1	6.5	8.0	7.1	7.5	7.7*					
MnO	0.10											
MgO	18.1(a)											
CaO												
Na_2O	0.51											
K_2O								0.200				
P_2O_5												
ppm												
Sc	17	12	13	15	13	14	15					
V												
Co	33	25	30	28	25	25	34					
Ni												
Rb												
Sr												
Y												
Zr	563	362	411	866	613	743	486		271	331	337	576
Nb												
Hf	12.4	8.64	9.24	19.7	14.1	17.1	11.1		6.4	7.5	8.1	14.3
Ba												
Th								4.05				
U								1.10				
Cs												
Ta												
Pb												
La												
Ce												
Pr												
Nd												
Sm												
Eu	1.6	1.3	1.4	2.1	1.6	1.6	1*					
Gd												
Tb												
Dy												
Ho												
Er												
Tm												
Yb												
Lu												
Li												
Be												
B												
C												
N												
S												
F												
Cl												
Br												
Cu												
Zn												
ppb												
Au												
Ir												
I												
At												
Ga												
Ge												
As												
Se												
Mo												
Tc												
Ru												
Rh												
Pd												
Ag												
Cd												
In												
Sn												
Sb												
Te												
W												
Re												
Os												
Pt												
Hg												
Tl												
Bi												
	(6)	(6)	(6)	(6)	(6)	(6)	(6)	(7)	(13)	(13	(13)	(13)

References and methods:
(6) Ehmann et al. (1975a,b); INAA, RNAA,; Zr values corrected for U fission (decreased less than 10 ppm) by Garg and Ehmann (1976a)
(7) Eldridge et al. (1975a,b); Gamma ray spectroscopy.
(13) Hughes and Schmitt (1985); INAA

Notes:
(#) erroneous data from computational error reported in Ehmann et al. (1975b)
(*) approximate
(a) clearly erroneously high; major element oxides without CaO and TiO_2 total 97%

Table 4: Compositions of groundmass in aphanites, from defocused beam microprobe analyses and clast subtraction. James (1976)

	Black aphanitic matrix (73215,243)		Gray aphanitic matrix (73215,245)		Schlieren-rich gray aphanitic matrix (73215,103)		Clast-poor aphanite (73215,103)	Black aphanite clast (73215,46,10)		Gray aphanite spheroid (73215,38,57)		Bulk matrix†	Bulk black aphanite clast† (73215,46,10)	Bulk gray aphanite spheroid† (73215,38,57)
	Average	Range	Average	Range	Average	Range	Average	Average	Range	Average	Range	Average		
SiO_2	46.4	45.5–47.3	46.5	45.2–45.9	46.9	46.0–47.6	46.3	47.7	47.3–48.3	46.8	46.6–47.5	46.4	45.6	45.9
TiO_2	1.00	0.78–1.15	1.09	1.02–1.14	1.04	0.88–1.15	0.86	0.96	0.87–1.03	0.95	0.77–1.18	0.7	1.1	0.8
Al_2O_3	19.0	18.1–20.2	19.0	18.7–19.3	18.0	17.3–18.7	18.0	18.1	16.9–19.2	20.0	18.8–20.8	20.6	19.8	20.7
FeO	8.26	7.70–9.10	8.27	7.94–8.54	8.73	7.96–9.15	8.56	7.89	7.24–8.56	6.86	6.37–7.80	7.30	8.13	6.94
MnO	0.10	0.08–0.12	0.09	0.07–0.11	0.13	0.12–0.15	0.08	0.09	0.07–0.11	0.07	0.04–0.09	0.104	0.106	0.093
MgO	11.6	9.74–12.5	12.8	12.7–13.0	12.0	11.2–12.3	13.5	12.4	11.5–14.0	11.8	11.0–12.9	11.6	12.0	11.8
CaO	12.0	11.6–12.5	11.9	11.7–12.2	11.8	11.3–12.2	11.4	11.6	11.0–12.2	12.2	11.6–12.6	11.9	11.5	11.4
Na_2O	0.76	0.66–0.95	0.64	0.61–0.67	0.62	0.56–0.77	0.63	0.57	0.48–0.66	0.61	0.53–0.66	0.50	0.52	0.52
K_2O	0.29	0.17–0.39	0.30	0.25–0.33	0.31	0.27–0.39	0.29	0.24	0.20–0.27	0.24	0.22–0.25	0.20	0.22	0.16
Cr_2O_3	0.15	0.07–0.20	0.16	0.14–0.20	0.19	0.15–0.23	0.17	0.22	0.19–0.24	0.15	0.14–0.16	0.25	0.25	0.21
P_2O_5	0.41	0.26–0.48	0.25	0.20–0.30	0.31	0.25–0.42	0.25	0.29	0.26–0.33	0.31	0.26–0.35	—	—	—
Number of analyses in average	14		4		7		2	7		7		11		

*Derived from broad-beam microprobe analysis of 100 μm spots (analyzed by G. H. Conrad and K. Keil, University of New Mexico); contributions from all clasts >5 μm across within each spot have been subtracted and the resulting corrected compositions have been normalized to 100%.

†Determined by atomic absorption spectrophotometry and instrumental neutron activation analyses (Blanchard *et al.*, 1976).

Table 5: Chemical analyses of clasts in 73215.

Split	,94	,32	,29,9	,29,9	,29,9	,29,9	,29,9	,46,25	,46,33	,43,3	,43 IV	,46,102	,46,102
wt%	a	b	c	c	c	c	c	d	d	e	e	f	f
SiO_2	44.47	44.71	45.9	46.6				44.1					
TiO_2	0.08		0.69	0.58				0.23					
Al_2O_3	30.99	31.2	25.6	25.4				25.6					
Cr_2O_3			0.130	0.146				0.124	0.123	0.015			
FeO	3.03	3.05	4.44	5.14				5.82	5.1	2.98			
MnO			0.062	0.077				0.067					
MgO	3.42	3.42	8.36	8.42				9.41					
CaO	17.21	17.24	13.9	14.1				13.8					
Na_2O	0.44	0.47	0.430	0.403				0.356	0.375	0.194			
K_2O	0.10	0.036	0.121	0.097				0.088		7.0			
P_2O_5													
ppm													
Sc			7.16	9.04				7.12	8.2	4.8			
V													
Co			13.7	13.2				30.7	32.7	2.10			
Ni			80	80	64			420	460				
Rb	1.88	0.29				2.43	2.48				255.5	1.77	1.76
Sr						167.0	167.2				158.0	154.3	154.8
Y	33.7	19.7											
Zr	184	79											
Nb	10.4	6.3											
Hf	3.15	1.96	3.1	2.2				1.5	1.4	25.6			
Ba	182	61											
Th	1.34	0.80	1.6	0.96				0.53	0.58	39.9			
U	0.33	0.36			0.360								
Ca													
Ta			0.3	0.2				0.3	0.16	5.4			
Pb	1.4	1.87											
La	10.1	4.2	8.70	6.24				2.61	3.52	42.9			
Ce	27	12	24.4	16.8				6.78	9.1	125			
Pr	3.2	1.54											
Nd	12.1	6.3											
Sm	3.40	1.82	3.88	3.08				1.04	1.53	19.0			
Eu	1.23	0.50	1.00	0.91				0.77	0.77	3.11			
Gd	4.12	2.05											
Tb	0.82	0.42	0.84	0.82				0.23	0.36	5.6			
Dy	5.60	2.71											
Ho	1.32	0.57											
Er	3.67	1.62											
Tm	0.61	0.27											
Yb	3.67	1.66	2.9	3.0				1.4	1.71	27.2			
Lu	0.57	0.26	0.413	0.405				0.225	0.273	5.3			
Li													
Be													
B													
C													
N													
S													
F													
Cl													
Br													
Cu													
Zn					2.0								
ppb													
Au					0.58								
Ir					1.78								
I													
At													
Ga													
Ge					47								
As													
Se					40								
Mo													
Tc													
Ru													
Rh													
Pd					2.1								
Ag					0.74								
Cd					19.4								
In					3.2								
Sn													
Sb													
Te													
W													
Re					0.167								
Os					2.3								
Pt													
Hg													
Tl					2.64								
Bi					0.44								
	(2)	(2)	(4,5)	(4,5)	(11)	(14)	(14)	(4,5)	(4)	(4,5)	(14)	(14)	(14)

References and methods:
(2) Bence et al. (1975); EMP/spark source mass spec.
(4) Blanchard et al. (1977a); INAA, AAS
(5) Blanchard et al. (1977b); INAA, AAS
(11) Morgan and Petrie (1979a,b); RNAA
(14) Compston et al. (1977a,b); ID/MS

Notes:
a not characterized
b spinel troctolite
c coarse-grained anorthositic gabbro
d fine-grained anorthostic gabbro
e felsite
f feldspathic polymict material

Table 5 continued: Chemical analyses of clasts in 73215.

Split	,94	,32	,29,9	,29,9	,29,9	,29,9	,29,9	,46,25	,46,33	,43,3	,43 IV	,46,102	,46,102
wt %	a	b	c	c	c	c	c	d	d	e	e	f	f
SiO_2	44.47	44.71	45.9	46.6				44.1					
TiO_2	0.08		0.69	0.58				0.23					
Al_2O_3	30.99	31.2	25.6	25.4				25.6					
Cr_2O_3			0.130	0.146				0.124	0.123	0.015			
FeO	3.03	3.05	4.44	5.14				5.82	5.1	2.98			
MnO			0.062	0.077				0.067					
MgO	3.42	3.42	8.36	8.42				9.41					
CaO	17.21	17.24	13.9	14.1				13.8					
Na_2O	0.44	0.47	0.430	0.403				0.356	0.375	0.194			
K_2O	0.10	0.036	0.121	0.097				0.088		7.0			
P_2O_5													
ppm													
Sc			7.16	9.04				7.12	8.2	4.8			
V													
Co			13.7	13.2				30.7	32.7	2.10			
Ni			80	80	64			420	460				
Rb	1.88	0.29				2.43	2.48				255.5	1.77	1.76
Sr						167.0	167.2				158.0	154.3	154.8
Y	33.7	19.7											
Zr	184	79											
Nb	10.4	6.3											
Hf	3.15	1.96	3.1	2.2				1.5	1.4	25.6			
Ba	182	61											
Th	1.34	0.80	1.6	0.96				0.53	0.58	39.9			
U	0.33	0.36			0.360								
Ca													
Ta			0.3	0.2				0.3	0.16	5.4			
Pb	1.4	1.87											
La	10.1	4.2	8.70	6.24				2.61	3.52	42.9			
Ce	27	12	24.4	16.8				6.78	9.1	125			
Pr	3.2	1.54											
Nd	12.1	6.3											
Sm	3.40	1.82	3.88	3.08				1.04	1.53	19.0			
Eu	1.23	0.50	1.00	0.91				0.77	0.77	3.11			
Gd	4.12	2.05											
Tb	0.82	0.42	0.84	0.82				0.23	0.36	5.6			
Dy	5.60	2.71											
Ho	1.32	0.57											
Er	3.67	1.62											
Tm	0.61	0.27											
Yb	3.67	1.66	2.9	3.0				1.4	1.71	27.2			
Lu	0.57	0.26	0.413	0.405				0.225	0.273	5.3			
Li													
Be													
B													
C													
N													
S													
F													
Cl													
Br													
Cu													
Zn					2.0								
ppb													
Au					0.58								
Ir					1.78								
I													
At													
Ga													
Ge					47								
As													
Se					40								
Mo													
Tc													
Ru													
Rh													
Pd					2.1								
Ag					0.74								
Cd					19.4								
In					3.2								
Sn													
Sb													
Te													
W													
Re					0.167								
Os					2.3								
Pt													
Hg													
Tl					2.64								
Bi					0.44								
	(2)	(2)	(4,5)	(4,5)	(11)	(14)	(14)	(4,5)	(4)	(4,5)	(14)	(14)	(14)

References and methods:
(2) Bence et al. (1975); EMP/spark source mass spec.
(4) Blanchard et al. (1977a); INAA, AAS
(5) Blanchard et al. (1977b); INAA, AAS
(11) Morgan and Petrie (1979a,b); RNAA
(14) Compston et al. (1977a,b); ID/MS

Notes:
a not characterized
b spinel troctolite
c coarse-grained anorthositic gabbro
d fine-grained anorthositic gabbro
e felsite
f feldspathic polymict material

Table 6: Clast allocation types in 73215; see Figure 22. From James and Blanchard (1976).

	Aphanitic lithologies							
Principal Investigator	Gray matrix	Black matrix	Heterogeneous black matrix	Schlieren-rich gray matrix	Light-gray matrix	Gray spheroids	Black aphanite clasts	Rind on ANT-suite clast
Anders	76(3) 9006,170(3)	9003,161(4)				38,57(2)	46,10(2) 46,19(2)	
Eglinton	73(3)	82(4)		128(2)				
Burns	21(3)	34(4)						
(Brecher)	65(3)	85(4)						
Compston		38,49(2)	157(2)	178(2)	46,45(2)	38,57(2)	46,10(2)	
		36,3(2)	258(2)			38,32(2)	46,19(2)	
Haskin	74(3)	161(4)	159(2)	177(2)	186(2)	38,17(2)	46,2—	46,25(2)
	46,33(2)	209(2)	184(2)		46,30(2)	38,32(2)	46,7(2)	
		262(2)			170(2)	38,57(2)	46,10(2)	
							46,19(2)	
James	228(3)	127(2)	282(2)	103(2)	46,37(2)	38,17(2)	46,2—	46,25(2)
	245(3)	243(4)	283(2)	106(2)		38,32(2)	46,7(2)	
		231(4)		107(2)		38,57(2)	46,10(2)	
				247(2)		121(2)	46,19(2)	
				238(2)			118(2)	
							120(2)	
Kaplan			156(2)					
			273(2)					
Kirsten	9001,73(3)	41(2)		9005,177(2)	46,44(2)	38,57(2)	46,10(2)	
		36,2(2)				38,32(2)	46,7(2)	
							46,19(2)	
Marti	33(2)	260–1, 263–8(2)						
Price	72(3)	162(4)		92(2)	88(3)			
Reed†		81(4)		136(2)				
Silver		213(2)						
Ehmann†	66(3)	160(4)		176(2)				
	68(3)	163—						
	172—	166(4)						
Taylor, S. R.†		90(4)		94(2)	140(2)			

*Numbering system is as follows: samples numbered 29,X, 36,X, 38,X, and 46,X were obtained by chipping of large consortium pieces in air and distributed by D. P. Blanchard; samples numbered 900X,Y are from pieces obtained by chipping in the SSPL and then further subdivided in the lab of a consortium member—the initial recipient has retained the split with the original specific number Y; all other samples are listed by NASA-assigned specific numbers. The number in parentheses after the specific number indicates the figure on which the subsample appears.

†Investigators who are not members of the consortium but who have analyzed samples from the rock.

‡These are not all lithologically equivalent nor are they from the same area of the rock.

ANT-suite clasts						Surface samples		
Coarser-grained anorthositic gabbro	Finer-grained anorthositic gabbro	Granulated troctolite	Spinel-bearing troctolitic basalt	Granulated feldspathic clast materials‡	Felsite clast	Exposed top	Partly buried side	Buried bottom
29,9(2)	46,25(2)		9007,170(2)	46,103(2)				
						152(2)		
29,9(2)	46,25(2)			46,102(2)	43(2)			
29,9(2)	46,25(2)	38,5—	170(2)	38,18(2)	43(2)	151(2)	185(2)	
	46,33(2)		38,23(2)	38,26(2)				
			38,33—	38,45—				
				46,5(2)				
29,9(2)	46,25(2)	121(2)	170(2)	118(2)	43(2)			
	46,33(2)	122(2)	38,23(2)	120(2)				
		124(2)	38,33—	46,5(2)				
		125(2)		46,105(2)				
		38,39(2)		46,13(2)				
				38,18(2)				
				38,45—				
				38,22(2)				
						146(2)	139(2)	
						147(2)		
29,9(2)	46,25(2)	38,39(2)		46,6(2)	43(2)			
	46,33(2)							
	46,25(2)							
				46,101(2)		27(2)		87(2)
		32(2)		49(2)				

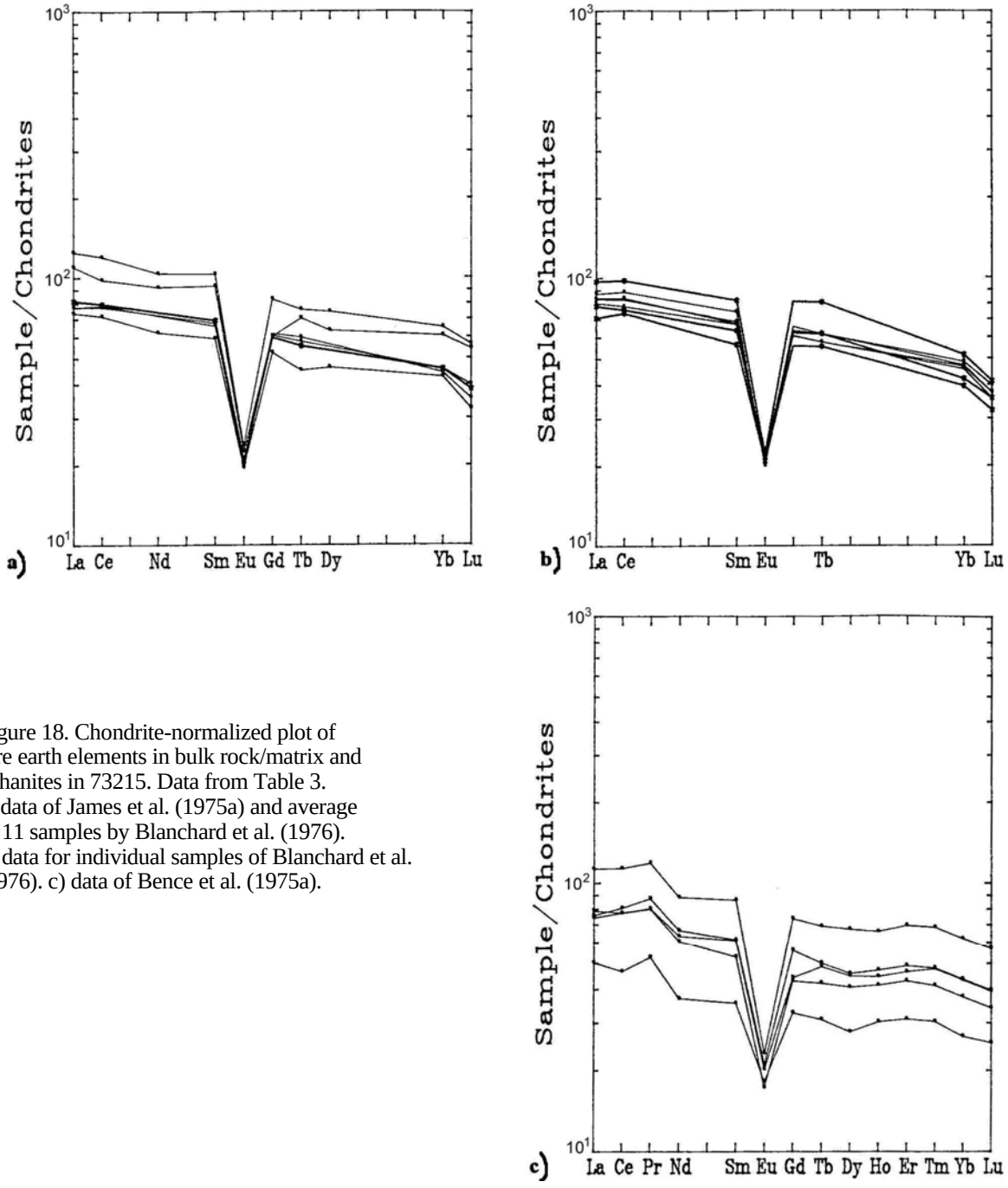

Figure 18. Chondrite-normalized plot of rare earth elements in bulk rock/matrix and aphanites in 73215. Data from Table 3. a) data of James et al. (1975a) and average of 11 samples by Blanchard et al. (1976). b) data for individual samples of Blanchard et al. (1976). c) data of Bence et al. (1975a).

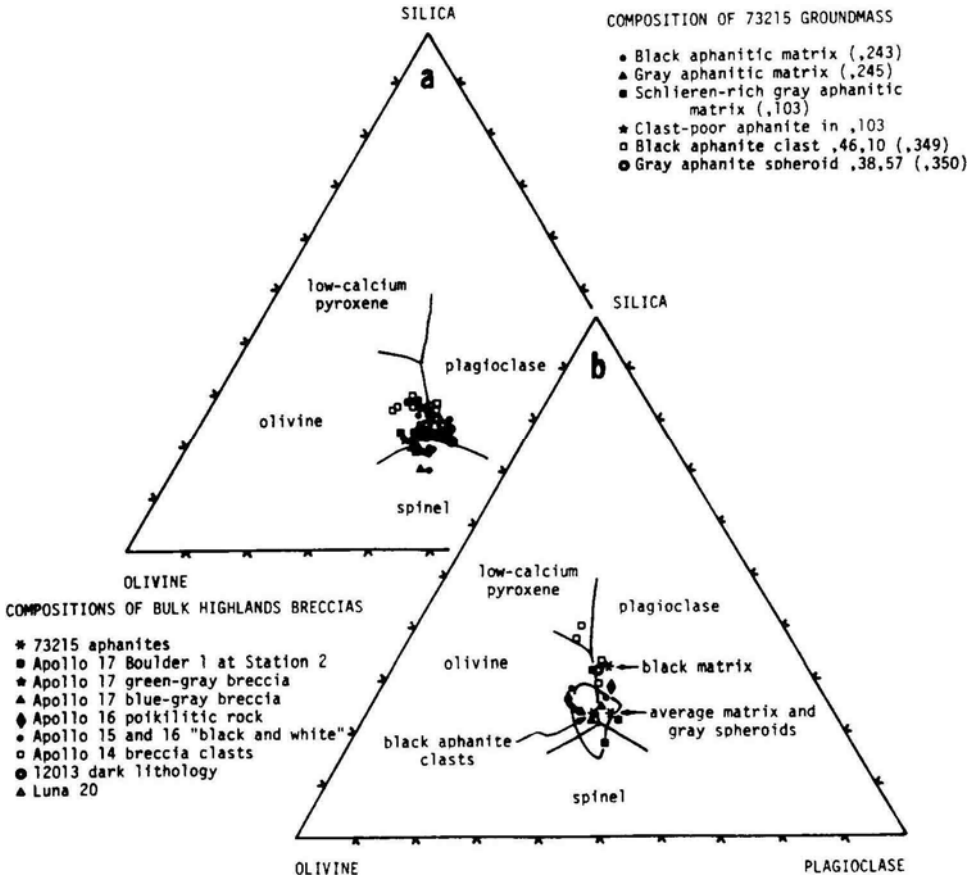

Figure 19. Compositions of groundmass melt in 73215 and other samples on silica-olivine-plagioclase plot. James (1976).

Several groups have reported analyses of "anorthositic gabbros" or feldspathic, granulitic impactite clasts in 73215. Blanchard et al. (1977a,b) reported that ,46,25 and ,46,33 were similar to each other and are similar to other feldspathic impactites such as 78155. They are somewhat different from ,29,9, which has higher rare earth elements and a negative Eu anomaly (Fig. 20) and also has high Cd and Sb (Morgan and Petrie, 1988). Clast ,45,25 is also high in meteoritic siderophiles (e.g., Ni more than 400 ppm), whereas 29,9 has much lower levels of meteoritic contamination. Gros et al. (1976) placed ,46,25 in meteoritic Group 3L; sample 29,9 was also Group 3 (Morgan and Petrie, 1988). Some other analyses in Table 5 may also be of similar materials, but accurate descriptions have not been retrieved.

Blanchard et al. (1977 a,b) reported analyses of other feldspathic breccias, some of which are probably polymict (Table 5, Figure 21). The high rare earths and continuous rare earth slopes of some samples are probably a result of matrix contamination. The fine-grained, igneous-textured spinelbearing troctolite analyzed appears to have indigenous rather than meteoritic siderophiles (Higuchi and Morgan, 1975 a,b) and roughly matches the 72417 dunite in the siderophile relative abundances (Morgan and Wandless, 1988). Bence et al. (1975) reported data for a spinel troctolite clast of undescribed nature; it is certainly feldspathic with fairly low incompatible element abundances (Fig. 21). Eckert et al. (1991 a,b) reported on the chemistry of an apparently cumulate spinel troctolite without tabulating the data. The sample has 28% $A1_2O_3$ and a positive Eu anomaly. The small dunite clast analyzed by the same group (Eckert et al., 1991 b) has low rare earth element abundances with a fairly flat rare

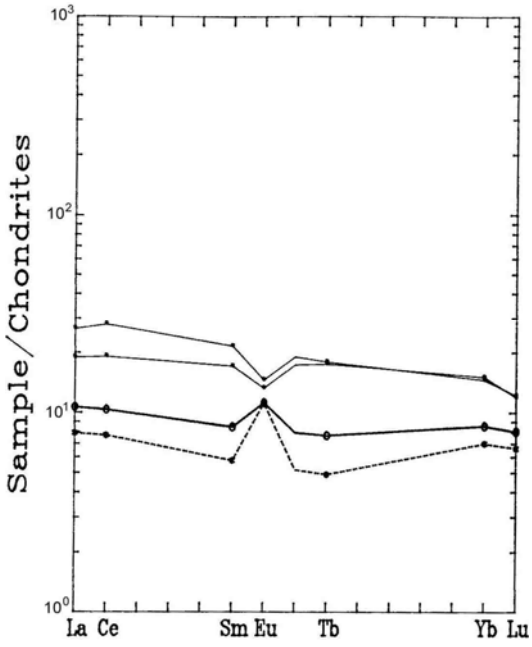

Figure 20. Chondrite-normalized plot of rare earth elements in feldspathic impactites (granulites, or "anorthositic gabbros") in 73215. Data from Table 5.

earth element pattern and only a small negative Eu anomaly; however, the mineral variability suggests that this sample is polymict, not pristine igneous. One of the two clasts analyzed by Bence et al. (1975) was described as spinel troctolite and is the most feldspathic of 73215 clasts analyzed; the other clast, not described, is similar but has twice the abundance of incompatible elements.

The felsite pieces analyzed were tiny (less than 14 mg). The sample is K-rich and poor in FeO and Na20, with high rare earth element abundances (La 130 x chondrites; Fig. 21). The pattern is V-shaped, and the chemistry suggestive of an origin that includes liquid immiscibility (Blanchard et al.,1977 b).

STABLE ISOTOPES

Sulfur isotope data for matrix samples were reported by James et al. (1975 a). The $s^{34}S$ o/oo values for two samples of interior heterogeneous matrix were 1.0 and 1.7 and for surface chips were 1.9 and 2.0. These values are like those of lunar crystalline rocks and unlike those of typical regoliths or regolith breccias.

RADIOGENIC ISOTOPES AND GEOCHRONOLOGY

Geochronological studies have been conducted on both aphanitic matrix and varied clasts in 73215. Because of the fine-grained nature of the aphanites, most of the work on them has been on the Ar-Ar system. The clasts and the melt groundmass have not equilibrated with each other in any of the investigated systems. The argon data clearly demonstrate incomplete degassing during the breccia-forming event and Ar loss appears to have been varied depending on particular thermal histories and clast types. Both stepwise heating and laser Ar studies have been conducted on 73215 materials.

Jessberger et al. (1976 a,b; 1977) and Staudacher et al. (1977) included several aphanitic matrix materials in their stepwise heating studies of 73215. They tabulated the data and produced release diagrams (Figs. 23 and 24; note the age axes use the "old" decay constants). The argon age data are summarized in Table 7, where the "new" decay constants are used. The results clearly demonstrate incomplete degassing, with the structure of the releases apparently resulting from combinations of old clastic material and melt. Few of the plateaus are very constant or very flat (Figs. 23, 24). Given that the age of the melt is probably best given by the age of the melted felsite clast within it (see below) and thus 3.87 +/- 0.01 Ga, then even claimed good plateaus such as that of gray matrix ,73,1, which produces an age of 4.09 +/-0.01 Ga must reflect undegassed class material. None of the samples analyzed are pure groundmass melt, and thus the "ages" yield only upper limits of the events that formed them (Jessberger et al., 1976a). Although the aphanitic melt spheroids and clasts give old "ages", the petrographic and chemical data strongly imply that these clasts and the matrix aphanites all formed in the same event, and thus these "ages" of up to 4.18 Ga (new constants) also reflect incomplete degassing of clasts. There is a reasonable correlation among aphanite samples of decreasing "age" with increasing K content, which may reflect the content of better-degassed felsite clasts (Jessberger et al., 1976). Jessberger et al. (1977) find it at

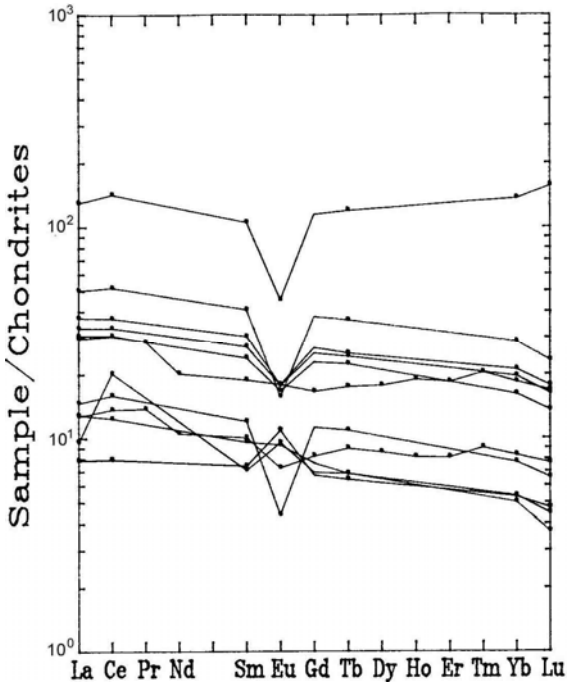

Figure 21: Chondrite-normalized plot of rare earth elements in felsite and feldspathic breccias in 73215. Data from Table 5.

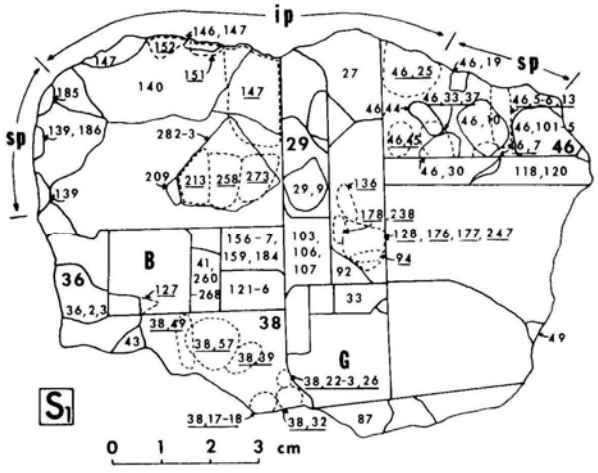

Figure 22: Map of slab sample locations and allocated material for 73215; see Table 6. (From James and Blanchard 1976).

least conceivable, however, that the data can be interpreted in a straightforward manner and that some of these clasts are indeed old melts.

Muller et al. (1977a,b) and Eichorn et al. (1978 a,b) conducted Ar isotopic studies on 73215 aphanitic materials using pulsed laser release of argon from polished surfaces. The method allows precise selection of the target through petrographic observation; the releases are from small areas (10-100 micron half-spheres) so individual small phases can be targeted. The method differs from step-wise heating in that all the gas is measured at once, because temperature control is not possible; thus the method is in essence K-Ar, not Ar-Ar. Pre-heating of the samples at 550-750°C (after irradiation, but before laser pulsing) was used to remove argon from unretentive phases and thus to single out gas from retentive phases that have greater chronological significance. Numerous small clasts in the matrix as well as groundmass melt were targeted. The data are reproduced in Tables 8 and 9, which are taken from Eichorn et al. (1978) who revised the older data from Muller et al. (1977a) with correction of the K/Ca ratios (Table 8). Fuller descriptions of the targets are given in the original papers.

Muller et al. (1977 a,b) analyzed clasts and groundmass in two matrix chips (Table 8), one a schlieren-rich gray matrix, the other just gray matrix, with about 50% recognizable clasts in a microsubophitic melt. The data indicate clearly that during the breccia-forming event degassing of argon was incomplete on a scale of tens of microns. The three groundmass age determinations agree within error at 4.01 Ga, but plagioclase clasts show variedly older ages and some clasts, including felsites, have younger ages (about 3.90 Ga). The most likely of possible alternative explanations is that the younger ages represent an upper limit to the

Table 7: Summary of argon ages for 73215 materials, using new decay constants. Jessberger et al. (1978).

Subnumber	Sample		K-Ar Age AE	^{40}Ar-^{39}Ar Plateau Age AE
43,3	felsite clast		3.83	3.87 ± .01
36,2	black	matrix	3.77	3.93 ± .01
41,1	black		3.93	3.99 ± .03
46,44	light gray		3.90	397 ± .01
73,1	gray	aphanites	4.03	4.09 ± .01
177,1	schlieren-rich gray		4.04	4.07 ± .04
38,32,5	gray spheroid		3.98	4.03 ± .01
38,57,4	gray spheroid		4.05	4.10 ± .03
46,7,3	vesicular black clast		3.92	3.97 ± .01
46,19,5	non-vesicular black clast	clast	3.97	4.03 ± .01
46,10,7	non-vesicular black clast	aphanites	4.08	4.18 ± .01
46,6,1	dark gray clast		4.05	4.11 ± .07
38,39,1,1	troctolite vein		3.90	3.95 ± .06
38,39,1,1	feldspathic clast		4.13	4.05 ± .05 4.22 ± .03
29,9,6	anorthositic gabbro clasts		4.10	4.00 ± .02 4.18 ± .01
46,25,5			4.07	4.02 ± .01 4.20 ± .01
46,33,4			4.09	4.02 ± .01 4.16 ± .01

age of the breccia-forming melt event (and not a subsequent heating event), and older ages represent incomplete degassing during that event. The groundmass melt "age" of 4.01 Ga then has no real chronological significance, and represents incomplete degassing of even the silicate liquid phase, or a still-appreciable content of very tiny, undegassed clasts, or gain of argon by the melt from the clasts during cooling. Eichorn et al. (1978) analyzed aphanitic clast material that was black, and which had given an anomalously old age by Ar-Ar (Jessberger et al., 1976a). The purpose was to establish the ages of various components of clasts and melt groundmass (Table 9). The results strongly support the suggestion that the black aphanite clast is cogenetic with the main matrix samples; a felsic glass clast is the same age as that of other felsic clasts and the breccia forming event, i.e. 3.89 Ga, and the groundmass itself gives a similar age. The older age of Jessberger et al. (1976 a) must clearly reflect the presence of undegassed clasts.

Compston et al. (1977 a,b) reported Rb-Sr isotopic data on six bulk matrix and five aphanitic clasts in 73215 (Table 10). The range in Rb/Sr results principally from differences in the Rb contents and reflects mainly a variation in felsite clast content. At breccia formation (about 3.83 Ga, new constants) there were small differences in $^{87}Sr/^{86}Sr$ ratios; data for the matrices are correlated along a mixing line that passes near though not exactly through the felsite data Mixing is evident, with the low Rb members consisting of feldspathic materials with low initial $^{87}Sr/^{86}Sr$ and material with higher initial ratios. The data shown in Fig. 25, which includes data for Boulder 1, Station 2, emphasizes such differences and demonstrates the lack of Sr isotope equilibration on a 1 cm to 1 mm scale. The age of the breccia-forming event cannot be determined directly from the aphanite data, but must be inferred from clast data, particularly the felsites, which give an age of 3.83 +/- 0.05 Ga (new constants). Figure 25 shows that many 73215 aphanites have model ages greater than 4.5 Ga; one possible explanation is volatile loss of Rb during melt formation, although it is not known whether the "excess -age component is the melt phase or a clast phase. Compston et al. (1977a) note that if the older Ar ages result from incomplete degassing and the older Rb-Sr model ages result from Rb loss, then there should be a reciprocal relationship between the Ar age and the K content of aphanites, but such a correlation is in fact weak, and degassing and volatilization must be complex.

James et al. (1975) reported data from a U, Th, and Pb isotopic study of black matrix material. On a concordia diagram the 73215 data fall within the field defined by other Apollo 17 melt breccias such as Boulder 1, Station 2 and the North Massif melt boulders (Fig, 26). The data plot very roughly along a chord with intersections at 4.4-4.5 and 4.0 Ga, suggesting old components strongly modified by outgassing during the breccia forming event. James et al. (1976) reported Nd isotopic data for a sample of black matrix (also plotted in a Figure in Lugmair et al., 1975). The $^{143}Nd/^{144}Nd$ of 0.51185 +/-0.00003 is lower than chondritic evolution, and the data require at least a two-stage evolution, with a stage very early in lunar history with Sm/Nd even lower than in the present breccia.

A fission track age for a whitlockite clast (James et al., 1975; Braddy et al. 1975a,b; and Goswami et al. 1976a,b) using a Lexan mapping technique is 4.05 (+0.05, -0.08) Ga, with uncertainties resulting from corrections for cosmic ray exposure. The age is in reasonable agreement as a compaction age for

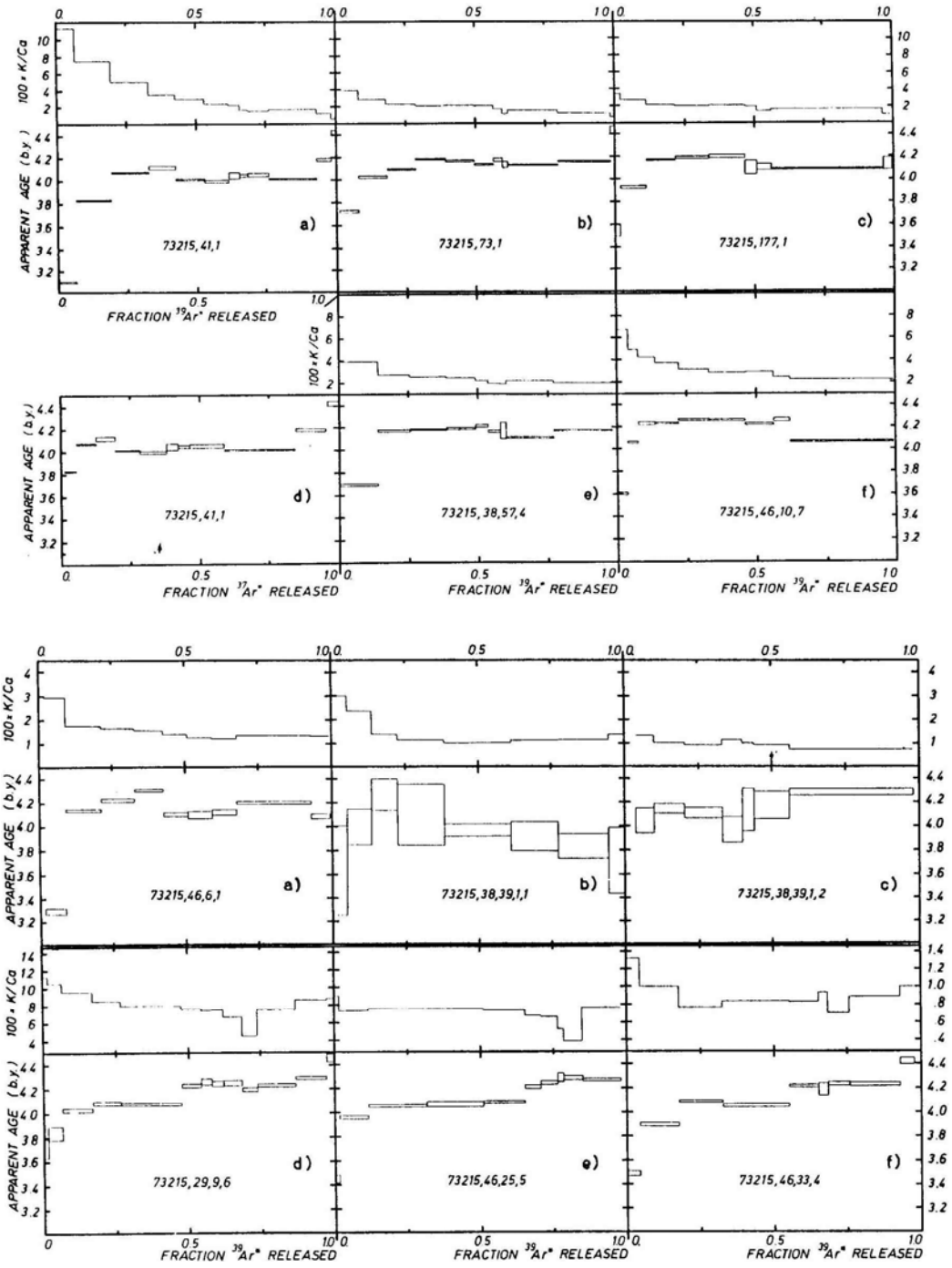

Figure 23: Ar release diagrams and ages for 73215 materials; ages are for old constants and should be reduced by about 0.06 Ga for new decay constants. Jessberger et al. (1977a). Key: Part 1, a) black matrix, b) gray matrix, c) schlieren-rich gray matrix, d) black matrix plotted against $^{37}Ar^{*}$, e) gray aphanite spheroid f) black aphanite clast. Part 2, a) dark gray aphanite clast, b) olivine in troctolite vein, c) feldspathic clast, d)-f) feldspathic granulites ("anorthositic gabbros").

Figure 24: Ar release diagrams and ages for 73215 materials; ages are for old constants and should be reduced by about OA6 Ga for new decay constants Jessberger et al. (1977a).

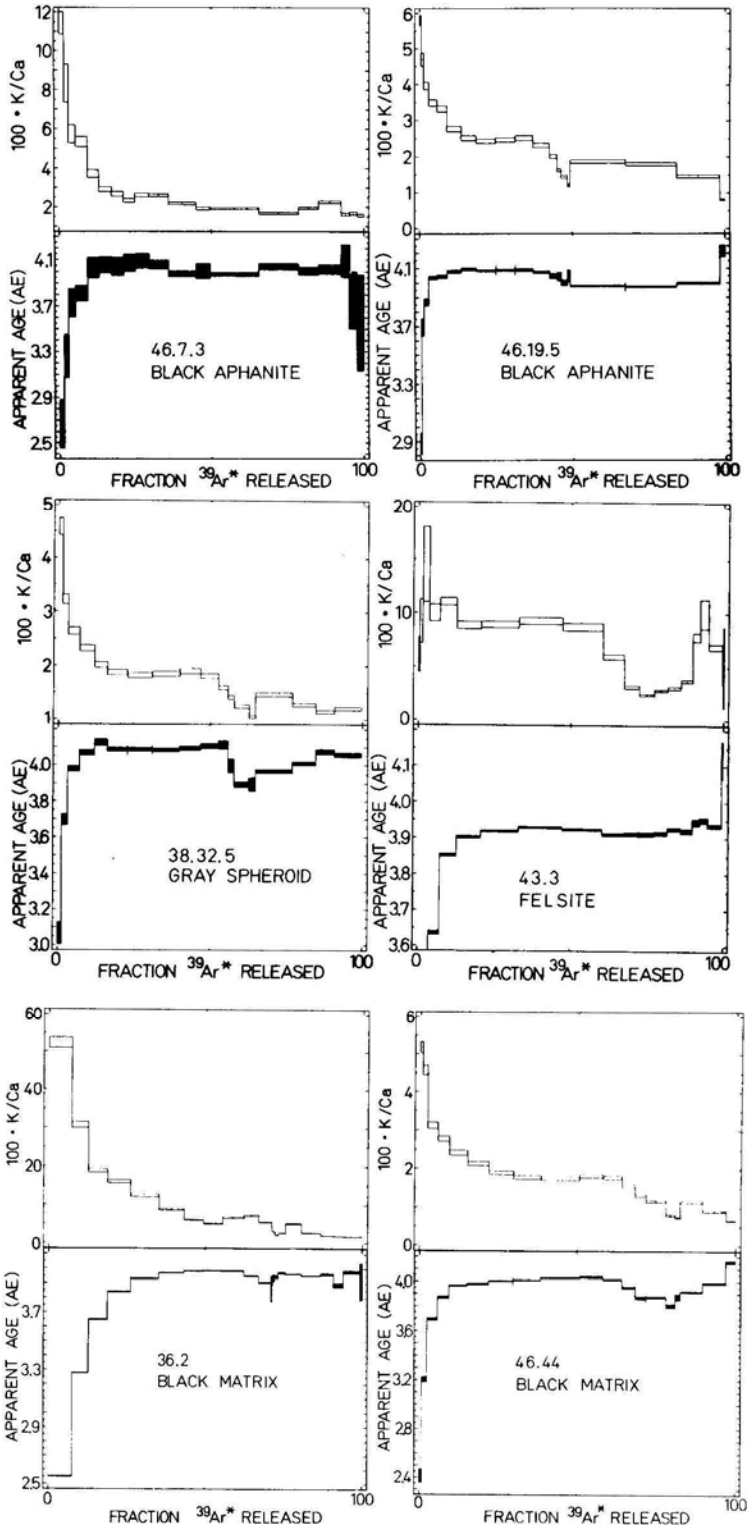

Table 8: Laser argon results for aphanitic matrix material in 73215; new decay constants
Originally from Muller et al. (1977ab), revised by Eichorn et al. (1978) in simplified form.

Material	K/Ca	$^{40}Ar_K/^{39}Ar_K$	Age (G.y.)
Matrix sample 73215,177 unheated			
Groundmass	.021	77.00	3.96
	±.001	±1.57	±.03
Matrix sample 73215,177 preheated to 550°C			
Groundmass	.021	79.70	4.01
	±.002	±3.98	±.07
Center of 0.28 mm plagioclase clast	.008	87.56	4.17
	±.001	±5.29	±.08
Centers of 29 40–125 μm plagioclase clasts	.011	84.01	4.10
	±.002	±2.28	±.04
0.24 mm clast of devitrified maskelynite	.012	85.56	4.13
	±.002	±3.04	±.05
Matrix sample 73215,131 preheated to 550°C			
Groundmass	.021	76.63	3.93
	±.001	±1.22	±.02
Groundmass in clast-poor matrix	.030	79.57	3.99
	±.001	±1.88	±.03
Granulated 0.4 mm core of 0.9 mm anorthosite clast	.007	71.18	3.81
	±.001	±2.14	±.04
Granulated 0.4 mm core of 0.9 mm anorthosite clast, repolished	.008	65.87	3.69
	±.001	±2.03	±.04
Recrystallized rim of 0.9 mm anorthosite clast	.009	78.22	3.96
	±.001	±2.31	±.04
0.4 mm clast of recrystallized anorthosite	.010	79.00	3.98
	±.001	±3.06	±.05
0.4 mm clast of recrystallized anorthosite, repolished	.011	80.98	4.02
	±.001	±2.32	±.04
0.15 mm clast of felsite (vermicular intergrowth of K-feldspar, quartz, and plagioclase)	1.328	82.34	4.04
	±1.328	±5.44	±.09
0.25 mm clast of felsic glass	2.788	75.18	3.90
	±.971	±1.84	±.03
0.25 mm clast of felsic glass, repolished	1.787	69.89	3.78
	±1.787	±.63	±.01
Matrix sample 73215,131 preheated to 750°C			
Granulated 0.4 mm core of 0.9 mm anorthosite clast	.007	74.13	3.89
	±.001	±1.12	±.02
0.25 mm clast of felsic glass	1.683	73.09	3.85
	±1.683	±0.55	±.01

[1]Data from Müller *et al.* (1977) recalculated using "new" preferred values for the isotopic composition of K, the decay constants, and the monitor composition (see text). K/Ca values have also been revised because the previously published values were in error.

Table 9: Laser argon results for black aphanite clast material and inclusions. Eichorn et al. (1978a).

Analysis Number	Material	Number of Pulses	^{40}Ar	$^{39}Ar^*$	$^{38}Ar^*$	^{37}Ar	$^{36}Ar^*$	K/Ca	$^{40}Ar_K/^{39}Ar_K$	Age (G.y.)
		Black aphanite clast 73215,46,10 preheated to 650°C								
1. (09131)	Groundmass	~100	525.5	6.87	3.91	107	4.79	.034	76.3	3.90
			±2.5	±.12	±.69	±9	±1.37	±.003	±1.4	±.03
2. (09133)	Groundmass	~100	554.0	7.45	5.34	116	7.81	.034	74.0	3.86
			±2.6	±.13	±.32	±4	±.76	±.002	±1.4	±.03
3. (01212)	Center of 0.25 × 0.40 mm plagioclase clast A	~35	232.6	2.85	1.61	241	1.21	.006	81.7	4.01
			±2.0	±.24	±.28	±28	±.49	±.001	±6.8	±.11
4. (01256)	Plagioclase clast A, repolished	60	777.4	9.58	5.60	612	2.69	.008	81.2	4.00
			±5.6	±.22	±.39	±72	±.45	±.001	±2.0	±.03
5. (01252)	75 × 100 μm felsic glass clast	13	244.2	3.23	.51	92	.09	.019	75.7	3.89
			±2.8	±.23	±.15	±61	±.09	±.013	±5.4	±.10
6. (01254)	130 μm clast of K-Ca-rich plagioclase	10	659.0	7.96	.12	19	.37	.216	82.8	4.03
			±3.6	±.23	±.12	±19	±.37	±.216	±2.4	±.04
7. (02033)	130 μm clast of K-Ca-rich plagioclase, repolished	8	1139.8	13.53	.34	39	.08	.185	84.3	4.06
			±6.1	±.46	±.26	±39	±.08	±.185	±2.9	±.05

[1]Information given in footnote to Table 1 applies to the data presented in this table as well. Blank levels for ^{40}Ar, ^{39}Ar, ^{38}Ar, ^{37}Ar, and ^{36}Ar were respectively: 4.8, .79, 28.0, 12.4, and 74.0 for measurements 1–2; and 6.8, 1.4, 2.5, 2.5, and 7.6 for the remaining measurements.
*^{39}Ar, ^{38}Ar, and ^{36}Ar corrected for n-induced contributions from Ca; ^{38}Ar also corrected for n-induced contributions from K.

Table 10: Rb-Sr isotopic data for 73215 whole-rock chip aphanite samples. Compston et al. (1977a).

			Rb	Sr	$^{87}Rb/^{86}Sr$	$^{87}Sr/^{86}Sr$
46,10.6 Black clast	A	22.2	4.83	137.1	.1016	.70551 ± 6
	B	10.1	5.02	143.7	.1007	.70551 ± 5
38,57.5 Gray spheroid	A	17.7	2.94	155.4	.0546	.70283 ± 8
	B	20.0	3.02	150.4	.0579	.70308 ± 5
157 Heterogeneous black matrix	A	24.0	5.96	139.8	.1231	.70649 ± 5
	B	25.4	5.67	138.6	.1179	.70626 ± 5
258 Heterogeneous black matrix	A	43.1	3.01	145.8	.0595	.70315 ± 5
	B	28.8	2.88	141.4	.0588	.70300 ± 5
46,45 Light-gray matrix	A	21.2	2.26	139.3	.0467	.70255 ± 6
	B	16.9	2.33	140.4	.0478	.70243 ± 5
178 Schlieren-rich gray matrix	A	25.3	3.46	138.9	.0719	.70390 ± 5
	B	23.5	3.24	139.9	.0669	.70355 ± 5
38,49 Black matrix	A	16.6	8.20	146.9	.1612	.70926 ± 7
	B	15.4	8.32	148.5	.1618	.70919 ± 5
46,102 Gray aphanite clast	A	6.21	3.27	131.2	.0720	.70369 ± 5
46,102 Gray aphanite clast	B	6.77	3.45	133.3	.0747	.70392 ± 5
38,32 Gray spheroid	A	15.7	7.16	147.2	.1405	.70785 ± 5
	B	19.4	6.87	148.8	.1333	.70739 ± 5
46,19 Black aphanite clasts		25.6	3.65	136.1	.0773	.70427 ± 5
36,3 Black matrix	I	22.2	58.2	165.4	1.0214	.75908 ± 5
	II	21.4	10.53	173.5	0.1753	.70969 ± 5

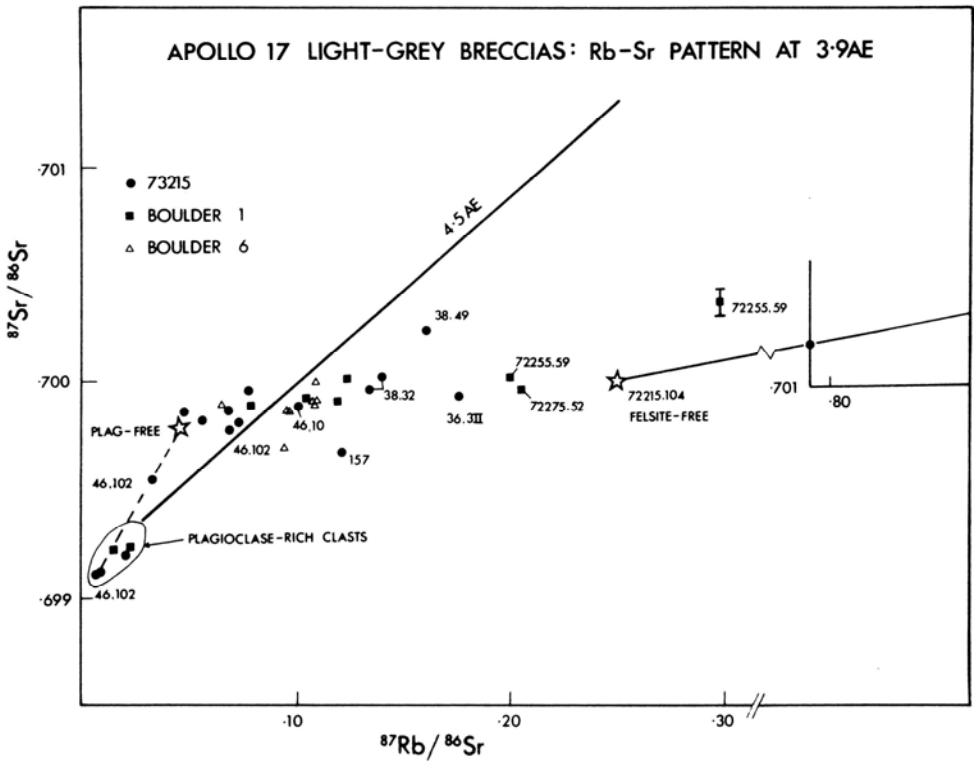

Figure 25: Sr evolution diagram for 73215 aphanite materials, after removal of radiogenic ^{87}Sr produced since 3.83 Ga (new constants). Compston et al. (1977a).

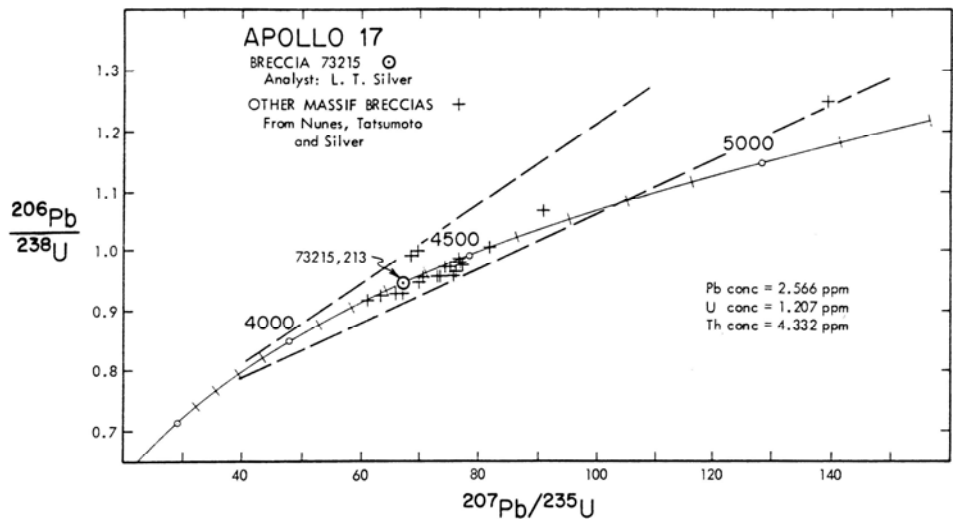

Figure 26: U-Pb concordia diagram for a 73215 matrix sample and other Apollo 17 breccia materials. James et al. (1975).

the breccia with results from the Ar and Sr systems.

The feldspathic impactite ("anorthositic gabbro") clasts were included in the argon studies of Jessberger et al. (1976 a,b) and Eichorn et al. (1978 a,b), and the strontium studies of Compston et al. (1977 a,b). Jessberger et al. (1976 a) stated that the releases (Fig. 23) for three samples had distinct two step plateaus: intermediate-temperature ones with ages of about 4.0 Ga (new constants) and high-temperature ones with ages of about 4.16-4.22 Ga (new constants). The K/Ca ratios do not show concomitant changes. The lower age
corresponds roughly with the breccia-forming event age, and is interpreted by Jessberger et al. (1977a) as thermal resetting by that event that left some material incompletely degassed. The older ages are thus lower limits on the age of the parent material. Two of these clasts were also studied by laser release methods, which also show a range of ages (Tables 11 and 12) (Muller et al. 1977a; Eichorn et al., 1978a,b). For the laser release studies, the samples were pre-heated as for the aphanites (above) and the ages are K-Ar on the more retentive phases. Small spots (30-60 micron half-spheres) were targeted, and ranged from cores of large and small plagioclases to small interstitial phases and rims. Plagioclase was the dominant phase being outgassed. The tabulated results show that cores of plagioclase crystals have higher ages (4.114.28 Ga, new constants) and recrystallized and apparent melt products have younger ages.(3.81-3.88 Ga). The pattern of dates is reasonably consistent with production by partial outgassing through grains and along grain boundaries when the clasts were incorporated in 73215, although not all of the observations fit such a process. The combined data for the two clasts set a lower limit of 4.26 Ga on the date of the high-temperature melting/recrystallization that affected them. The alternative that the melting event in the clast took place at about 4.0 Ga and that incorporation into 73215 had only minor effects is an unpreferred alternative explanation.

Compston et al. (1977 a,b) performed Rb-Sr isotopic studies on separates from two of the feldspathic granulites ("anorthositic gabbros") (Table 13, Fig. 27). Sample 29,9 has enough dispersion among plagioclase, olivine, and bulk rock to define an imprecise isochron at 4.18 +/- 0.31 Ga (new constants) with an initial $^{87}Sr/^{86}Sr$ of 0.69918 +/-0.0016. There is inadequate dispersion among the analyzed phases from 45,25 to define an isochron, although the data is consistent with the 29,9 isochron. Model ages based on BABI are about 4.3 Ga and supposedly constitute older limits on the age of the observed melting. If the systems were not entirely closed during incorporation into 73215, then the olivine model age of 29,9 might be a better estimate of its age; such a model age is 4.5 +/-.2 Ga, hence the impactite could be very old.

Other feldspathic and troctolitic clasts were analyzed in the argon and the strontium studies. Jessberger et al. (1976 a) analyzed a feldspathic clast that gave results similar to those of the feldspathic impactites (Fig. 23), with an older, higher temperature plateau and a younger, lower temperature plateau. Olivines picked from a stringer or vein do not give a good plateau and the errors are large because of the small amount of K in the sample. The spectrum shows a steady decrease in ages with temperature, possibly a result of recoil from included material, and the overall age is low, less than 4.0 Ga. Several of the fragments in the melt analyzed using laser release by Muller et al. (1977a,b) were feldspars or feldspathic materials and gave a variety of ages from 4.17 Ga to 3.69 Ga (Table 8). The sample of feldspathic material analyzed for Rb-Sr isotopes by Compston et al. (1977a,b) (Table

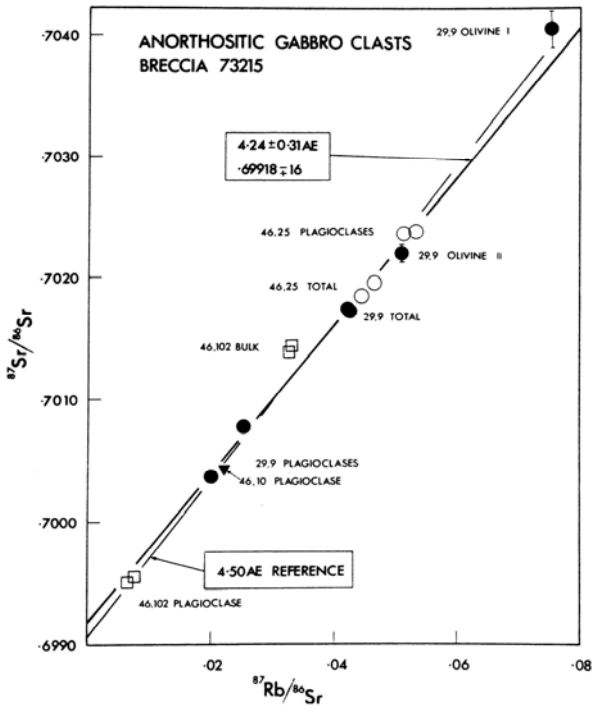

Figure 27: Strontium evolution diagram for feldspathic impactite and granulated feldspathic material in 73215. Calculated ages are for the old decay constants. Compston et al. (1977a).

Table 11: Laser argon release data for feldspathic impactite,46,25 (new constants). Eichorn et al. (1978a).

Analysis Number	Material	Number of Pulses	^{40}Ar	$^{39}Ar^*$	$^{38}Ar^*$	^{37}Ar	$^{36}Ar^*$	K/Ca	$^{40}Ar_K/^{39}Ar_K$	Age (G.y.)
	Sample 73215,46,25 preheated to 650°C									
1. (10184)	Centers of two 0.3 mm relict cores, grains A + B	~80	938.4 ±4.4	9.69 ±.09	4.36 ±.39	264 ±27	7.10 ±.67	.019 ±.002	96.5 ±1.0	4.28 ±.01
2. (01181)	Intermediate zone in relict core of grain A (after re-polishing)	36	431.8 ±2.8	4.76 ±.22	3.36 ±.45	362 ±62	2.28 ±.32	.007 ±.001	90.7 ±4.2	4.18 ±.06
3. (01191)	Intermediate zone in relict core of grain B (after re-polishing)	34	508.4 ±3.5	5.70 ±.21	3.54 ±.45	412 ±46	2.37 ±.61	.007 ±.001	89.1 ±3.4	4.15 ±.05
4. (12222)	0.3 mm relict core of grain C	67	467.7 ±2.7	5.30 ±.21	3.52 ±.27	380 ±37	2.59 ±.39	.007 ±.001	88.2 ±3.6	4.14 ±.06
5. (10186)	Eight 0.13–0.20 mm relict cores, grains E-L	~100	1003.0 ±2.4	11.55 ±.15	7.90 ±.73	561 ±11	8.91 ±.52	.011 ±.001	86.7 ±1.2	4.11 ±.02
6. (01185)	Five 0.06–0.10 mm relict cores, grains M-Q	42	385.2 ±3.9	4.36 ±.22	2.79 ±.26	265 ±31	2.02 ±.50	.009 ±.001	88.2 ±4.6	4.14 ±.07
7. (01174)	Core-rim boundary of grain C (after repolishing)	~75	521.0 ±4.8	6.33 ±.24	4.24 ±.21	463 ±66	2.59 ±.50	.007 ±.001	82.4 ±3.2	4.03 ±.05
8. (01183)	Rim of grain A (after repolishing)	35	517.6 ±3.6	6.31 ±.21	4.27 ±.52	480 ±54	2.61 ±.68	.007 ±.001	82.0 ±2.8	4.02 ±.05
9. (01176)	Rim of grain C (after repolishing)	30	488.8 ±5.8	5.84 ±.23	3.38 ±.26	435 ±52	2.69 ±.27	.007 ±.001	83.7 ±3.4	4.05 ±.06
10. (01195)	Rims of five grains (M-Q) containing relict cores	~55	415.7 ±2.5	5.06 ±.22	2.84 ±.24	342 ±55	1.24 ±.22	.008 ±.001	82.2 ±3.6	4.02 ±.06
11. (10191)	Centers of 0.1 mm recrystallized grains plus rims of grains A and B	~100	838.7 ±3.6	10.43 ±.15	7.27 ±1.15	541 ±6	7.32 ±1.26	.010 ±.001	80.3 ±1.2	3.99 ±.02
12. (10193)	Edges of grains bordering olivine	~100	868.6 ±2.6	11.76 ±.15	10.19 ±.62	604 ±15	12.02 ±.67	.010 ±.001	73.6 ±1.0	3.85 ±.02
13. (01197)	Edges of grains bordering olivine	~55	1014.0 ±4.4	14.06 ±.43	8.73 ±.49	895 ±164	5.29 ±.61	.008 ±.002	72.1 ±2.2	3.81 ±.04
14. (10188)	Small grains plus pyroxene in oikocrysts	~120	499.0 ±3.2	6.60 ±.12	6.95 ±.73	438 ±14	7.62 ±.70	.008 ±.001	75.4 ±1.4	3.88 ±.03
15. (10182)	Small grains plus pyroxene in oikocrysts	100–120	1102.5 ±8.5	15.15 ±.19	16.72 ±.65	938 ±20	24.15 ±.74	.009 ±.001	72.3 ±1.2	3.82 ±.02
	Sample 73215,46,25 preheated to 850°C									
16. (01262)	Edges of grain bordering olivine	68	726.3 ±3.7	8.75 ±.22	5.64 ±.21	498 ±57	3.27 ±.68	.009 ±.001	83.0 ±2.1	4.04 ±.04
	Sample 73215,46,25 preheated to 900°C									
17. (02013)	Center of 0.25 mm relict core of grain D	59	787.1 ±2.9	9.12 ±.23	4.44 ±.26	493 ±94	2.77 ±.54	.010 ±.002	86.3 ±2.2	4.10 ±.03
18. (01311)	Edge of relict core of grain A (after second repolishing)	55	595.3 ±2.7	6.30 ±.24	4.00 ±.31	587 ±63	3.25 ±.43	.006 ±.001	94.4 ±3.7	4.25 ±.05
19. (02031)	Rim of grain A (after second repolishing)	42	263.6 ±2.5	2.88 ±.21	1.86 ±.28	161 ±49	1.31 ±.58	.009 ±.003	91.5 ±6.8	4.20 ±.10
20. (02015)	Rim of grain D	36	408.9 ±2.4	4.44 ±.22	2.06 ±.11	359 ±53	1.59 ±.56	.007 ±.001	92.0 ±4.6	4.21 ±.07
21. (01313)	Edges of grains bordering olivine	57	426.2 ±3.1	4.73 ±.21	4.44 ±.56	464 ±63	3.12 ±.54	.005 ±.001	90.1 ±4.1	4.17 ±.06
22. (02011)	Small grains plus pyroxene in oikocrysts	59	254.8 ±2.1	2.75 ±.22	2.43 ±.32	257 ±41	.55 ±.43	.006 ±.001	92.5 ±7.5	4.21 ±.11

[1]Values are in 10^{-12} cm^3 STP; all values are corrected for blank. As the volume of material melted by each laser pulse is somewhat variable, we have not attempted to estimate gas concentrations in the rock sample (see text). Blank levels for ^{40}Ar, ^{38}Ar, ^{37}Ar, and ^{36}Ar were, respectively: 4.8, .79, 28.0, 12.4, and 74.0 for measurements 1, 5, 11, 12, 14, and 15; and 6.8, 1.4, 2.5, 2.5, and 7.6 for the remaining measurements. The blank is mainly the mass spectrometer tube background; the change in blank values was correlated with a change of the mass spectrometer multiplier and the accompanying bake outs. The blank for ^{40}Ar was variable by a factor of about 2; variation in the ^{39}Ar blank for the first set of measurements was $\pm 0.04 \times 10^{-12}$ cm^3 STP and for the second set of measurements was $\pm .2 \times 10^{-12}$ cm^3 STP. Gas samples in which the level of the ^{39}Ar from the rock was less than twice the blank level were found to give unreliable results so we have not reported analyses of such samples. Uncertainties reported in the ages are one standard deviation and indicate precision only, to facilitate intercomparison of the data; the absolute uncertainty is 0.02 G.y. (1σ).

*^{39}Ar, ^{38}Ar, and ^{36}Ar corrected for n-induced contributions from Ca; ^{38}Ar also corrected for n-induced contributions from K.

Table 12: Laser argon release data for feldspathic impactite 29,9 (new constants).
Ekhorn et al. (1978a). Data revised from Muller et al (1977a).

Material	K/Ca	$^{40}Ar_K/^{39}Ar_K$	Age (G.y.)
Sample 73215,29,9 unheated			
~0.4 mm relict core of ~0.8 mm grain	.012 ±.001	90.16 ±1.97	4.21 ±.03
Sample 73215,29,9 preheated to 550°C			
~0.4 mm relict core of ~0.8 mm grain	.006 ±.001	98.53 ±5.62	4.36 ±.08
~0.4 mm relict core of ~0.8 mm grain	.006 ±.001	95.21 ±3.88	4.30 ±.06
~0.4 mm relict core of ~0.8 mm grain	.007 ±.001	97.75 ±5.84	4.35 ±.08
Three ~0.2 mm relict cores in ~0.6 mm grains	.010 ±.001	95.79 ±3.00	4.31 ±.04
Centers of 48 .075-.230 mm melt-derived grains	.008 ±.001	82.29 ±2.10	4.07 ±.03

[1]Data from Müller *et al.* (1977) recalculated using "new" preferred values for the isotopic composition of K, the decay constants, and the monitor composition (see text). K/Ca values have also been revised because the previously published values were in error.

Table 13: Rb-Sr data for clasts of feldspathic impactite (anorthositic gabbro), granulated feldspathic material, and the felsite from 73215. Compston et al. (1977a).

		Weight (mg)	Rb ppm	Sr ppm	$^{87}Rb/^{86}Sr$	$^{87}Sr/^{86}Sr$
A. 29,9	A	19.0	2.43	167.0	.0420	.70175 ± 5
1. total-rock	B	21.1	2.48	167.2	.0427	.70173 ± 5
2. plagioclase	A	5.0	1.45	208.6	.0201	.70038 ± 5
	B	6.2	1.63	185.9	.0253	.70078 ± 6
3. olivine	I	2.1	.40	15.45	.0755	.70406 ± 23
olivine	II	5.3	.70	39.2	.0510	.70220 ± 8
B. 46,25	A	16.8	2.21	143.4	.0444	.70185 ± 5
1. total-rock	B	21.1	2.31	143.5	.0465	.70195 ± 6
	A	5.6	3.55	193.1	.0531	.70238 ± 5
2. plagioclase	B	5.0	3.22	181.0	.0513	.70237 ± 8
C. 46,102 feldspathic	A	23.7	1.77	154.3	.03316	.70144 ± 5
material	B	25.9	1.76	154.8	.03278	.70139 ± 5
2. plagioclase	A	3.00	0.46	199.8	.00666	.69950 ± 5
	B	2.52	0.56	207.2	.00777	.69955 ± 5
D. 46,10 plagioclase fragment		4.1	1.55	202.4	.0221	.70043 ± 5
E. 43,IV felsite chip		1.62	255.5	158.0	4.666	.96616 ± 6
43,III glass concentrate		0.55	252.0	91.9	7.910	1.14662 ± 8
43,II grey fraction		1.19	290.0	156.4	5.350	1.00460 ± 8
43,I white fraction		0.84	342.8	213.4	4.634	.96423 ± 5

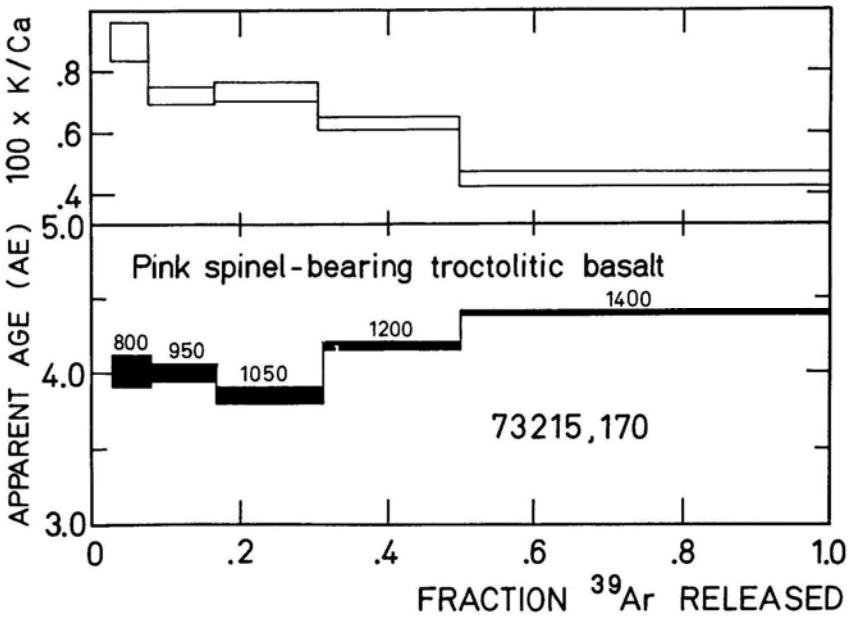

Figure 28: Apparent age and K/Ca spectra for a pink-spinel bearing troctolitic basalt in 73215. Jessberger et at (1979).

12) is probably polymict and might contain some 73215 matrix material. Its bulk analysis falls significantly above the feldspathic impactite isochron, and even above the 4.44 Ga reference isochron through BABI. In contrast, separated plagioclase falls below the feldspathic impactite isochron.

Jessberger et al. (1979) reported argon temperature release data for a clast of pink spinel-bearing troctolitic basalt (Fig. 28). This clast has been interpreted to contain indigenous, not meteoritic, siderophiles, and to have first crystallized rapidly and later to have suffered partial granulations and recrystallization, and then fragmentation. The age spectrum shows a two-step pattern similar to that of the feldspathic impactites, with an upper age of 4.46 +/- 0.04 Ga which must be a minimum age for the melting. The younger age of about 3.94 +/- 0.07 Ga is in agreement with the age of breccia - formation.

The felsite clast ,43,3 was analyzed by stepwise argon release by Jessberger et al. (1977a,b), and gave a good plateau at 3.86 +/-0.01Ga (new constants). The felsite was molten at the time of incorporation, so this age dates that of resetting of the felsite rather than its primary crystallization age; it is also the best definition of the age of the melt and breccia formation. Rb-Sr isotopic data (Compston et al., 1977a,b) for the same felsite (Table 13 and Figure 29) give an age of 3.84 +/- 0.05 Ga (new constants), in good agreement with the argon age. The slope of the isochron is controlled largely by the melted brown glass, and the age is that of the aggregation. The Rb-Sr model age of a "total-rock" chip gives a maximum crystallization age of 3.94 Ga. Felsic glasses analyzed in the laser argon studies also give ages in the 3.85 +/- 0.05 Ga range (Muller et al., 1977 a,b; Eichorn et al., 1978 a,b).

RARE GAS AND EXPOSURE

Rare gas analysis shows that trapped solar wind gases are essentially absent from 73215 (James et al., 1975a). Trapped Ne and Ar are less than 3 x 10^{-8}cc/g. James et al. (1975x) reported a Kr-Kr exposure age of 243 +/-7 Ma for black matrix (both Kr and Xe are dominantly from in situ-produced spallation and neutron-capture). ^{38}Ar exposure ages for three matrix chips reported in the same study are about the same: 185, 217, and 227 +/- 30 Ma. A moderate amount of shielding during irradiation is indicated by the data, on average about 10-15 cm of rock or soil. The data can be interpreted as dominantly a simple exposure history with one irradiation of about 243 Ma, or a more complex multi-stage irradiation; the latter seems less likely.

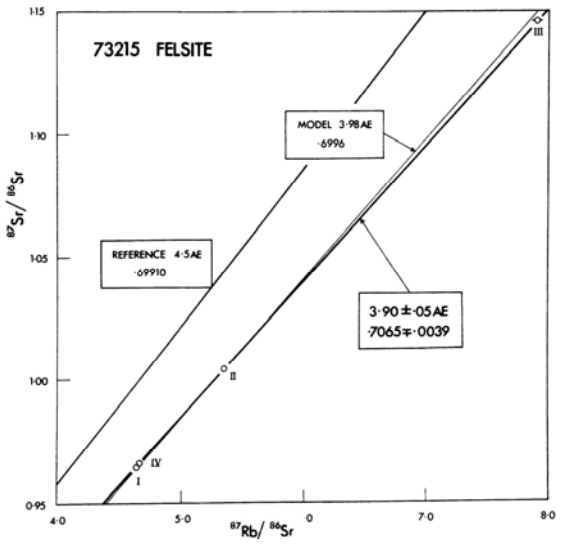

Figure 29: Internal Rb-Sr isochron for a felsite clast in 73215. Age stated is for old decay constants; new constant gives 3.84 +/- 0.05 Ca for the age of the felsite. Compston et al. (1977a).

Jessberger et al. (1977a; 1978a) reported ^{38}Ar cosmic ray exposure ages for several matrix and clast samples, including aphanitic clasts, feldspathic impactite clasts, and the felsite. All have the same exposure within uncertainty and average 244 +/-9 Ma, very close to the reported Kr-Kr ages. The ^{38}Ar exposure age for the pink spinel troctolitic basalt reported by Jessberger et al. (1979) at 256 +/-10 Ma is also in agreement within uncertainty.

O'Kelley et al. (1974 a,b) reported cosmogenic nuclide data for the bulk rock 73215, measured soon after splashdown. Their discussion mainly concerns the August 1972 solar flare event. 73215 appears to have been at least partly shielded from that flare, having low ^{54}Mn, ^{56}Co, and ^{46}Sc compared with other nuclides. Yokoyama et al. (1974) used the saturation of ^{26}A1 and ^{22}Na data to determine that the rock had had an exposure of at least a few million years.

Hutcheon et al. (1974b) measured track densities in 73215 and suggested that it had had a very complex irradiation history. The exposed surfaces are saturated with impact pits (according to Horz), hence at least a million years of exposure is suggested; the bottom had no craters, so there was no turnover in that time frame. However, the track density profile from the top to the bottom is virtually flat: 5 x 10^6t/cm^2 at 1.6 cm; 4.0 x 10^6t/cm^2 at 4.8 cm; and 3.7 x 10^6t/cm^2 at 6.7 cm. A long irradiation (more than 50 Ma) in a different orientation at a few centimeters depth is required, with the prediction of a long spallation age (which is in fact the case). Hutcheon et al. (1974 b) found no solar flare track density gradient near the surface of the sample measured. Nord and James (1977 a) also found track densities consistent with those of Hutcheon et al. (1974 b); one quartz grain showed higher densities that are probably a result of an adjacent U-Th-rich phase. Braddy et al. (1975 a,b) and Goswami et al. (1976 a,b) used such track data to estimate the compaction age of 73215 (see RADIOGENIC ISOTOPES AND GEOCHRONOLOGY section, above).

PHYSICAL PROPERTIES

Housley et al. (1976) made ferromagnetic resonance studies of 73215 and established that it did not have the FMR intensity characteristic of glassy agglutinates.

A detailed study of the magnetic properties of 73215 was made by Brecher (1975, 1976 a,b,c; also partly reported in James et al. 1975 a,b). She concluded that there are intimate interrelationships between the dominant petrographic features and the magnetization behavior that she terms textural remanent magnetism. The samples used were two cubes (3.4 g and 1.9 g) from 5 centimeters apart and mutually oriented. Both were aphanitic matrix materials, one black and one gray. Small chips of similar material were subjected to thermomagnetic analysis. The average Fe^O (0.121 and 0.15 wt%) and Fe^{2+} (6.31 and 6.35 wt%) of the cubes show the low degrees of reduction typical of crystalline highlands rocks and the sample show no evidence of a previous regolith history. Multi-domain metal grains dominate the magnetic behavior and the thermomagnetic analyses establish that they have meteoritic Ni.

The initial magnetic moments (Natural Remanent Magnetization, or NRM) were similar in the cubes as received and decayed only a little in two months storage in a zero field; thus acquisition of a viscous remanence from earth's field is probably negligible. The cubes were subjected to standard AF demagnetization (Fig. 30); the NRM is rather soft. The micro-coercivity spectra of both

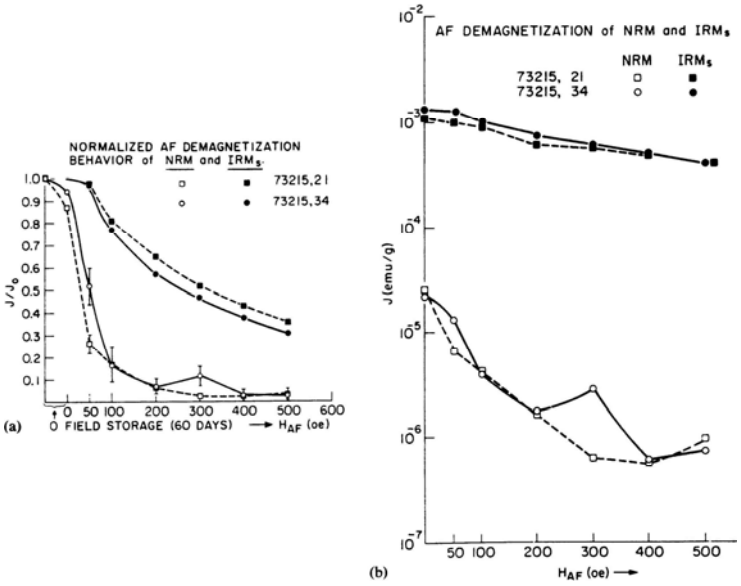

Figure 30. Absolute (a) and normalized (b) demagnetization curves of natural and saturation remanence in two cubes of 73215 matrix. (Brecher 1976b).

NRM and saturation remanence are similar in the two samples, with the saturation remanence about 50x the NRM. Figure 31 summarizes the directional changes. A stable and possibly primordial NRM should show directional convergence. The initial NRM directions of the two samples are different (points marked 0 in Fig. 31), in fact almost reversed. Cleaning in high fields results in oscillations with directions close to shear or other planes. Both the initial and convergence directions of magnetization are distinctly different in the two matrix cubes.

Thermomagnetic curves are reproduced as Figure 32. The samples were heated to 850 degrees C. The reproducible thermal hysteresis loops show that no chemical changes took place. The two samples are nearly identical, and the major phase is kamacite. The transformation temperature (gamma to alpha) corresponds with a Ni content of about 5%; the cooling behavior indicates that only 1% of the metal is pure Fe^{o}. Some low temperature inflections probably result from sulfides. Full magnetization curves and hysteresis loops were obtained for the two cubes (Figure 33), from which the Feo and Fe2+ contents are determined The average values of the hysteresis parameters (Table 14) confirm the predominance of multi-domain magnetic grains.

Brecher (1976b) measured the magnetic anisotropy by three different methods to detect the presence of the magnetic fabric implied by the directional behavior of the NRM. She used high-field anisotropy, where a comparison of the derived hysteresis loop parameters for the orthogonal directions indicates that both cubes are magnetically anisotropic. The anisotropy differs in sense and magnitude for each magnetic parameter. Anisotropy in the acquisition of anhysteric remanent magnetization (ARM) indicates that both samples have anisotropy in the same sense but to different degrees; the actual value for the degree of anisotropy is probably meaningless. The qualitative conclusion may be drawn that the gray matrix sample has a more pronounced magnetic fabric. Low-field anisotropic susceptibility also shows that the two breccias are magnetically anisotropic, and probably as a result of a magnetic fabric mimetic to the observed rock fabric. Brecher (1976a,b,c) discusses in some detail the model of textural remanent magnetism.

PROCESSING AND SUBDIVISIONS

Following separation of a few small chips, 73215 was sawn in late 1973, producing end pieces (,8, 140 g; and ,9, 644 g) and a slab (,10) about 1.5 cm thick (Fig. 2). Because of the complex structure of the rock, lithological maps were constructed to assist processing and allocation correlations (Figs. 4 and 22) for the consortium study led by 0. James. The slab was greatly subdivided by sawing (Fig. 22). A large number of thin sections from several pieces were cut from this rock, and allocations for many

types of study were made. In 1989 a further slab was cut from end piece ,9, which is now 372 g. This slab piece broke into pieces and allocations were made of clasts for chemical and petrographic studies.

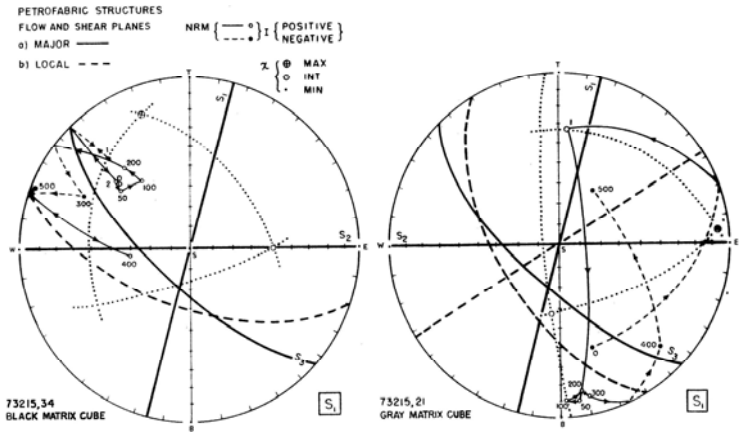

Figure 31: Directional behavior of NRM and the orientation of the magnetic susceptibility ellipsoid relative to petrofabric features of the two cubes from 73215. Brecher (1976b).

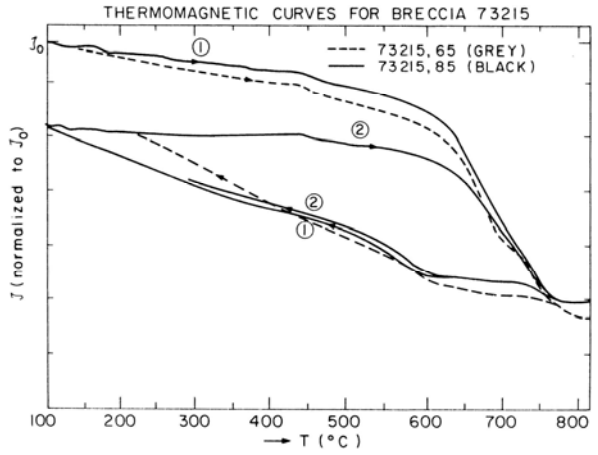

Figure 32: Thermomagnetic behavior for the cubes from 73215; Curves (1) are heating and (2) are cooling. Brecher (1976b).

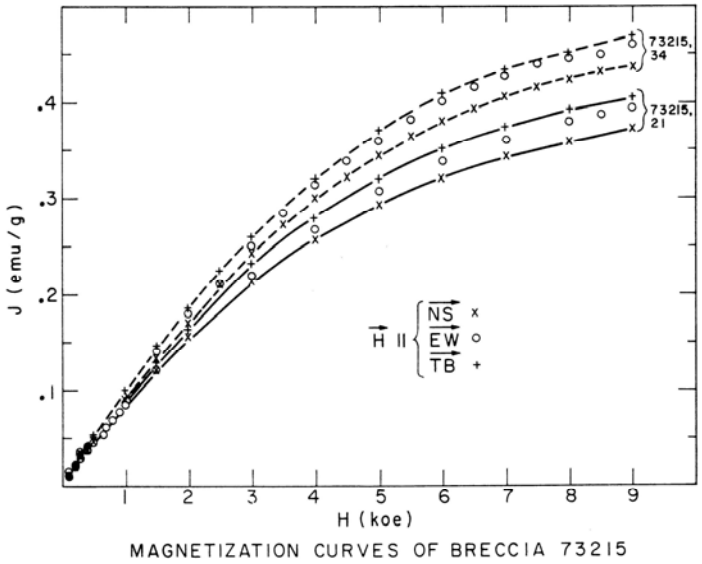

Figure 33: Sets of magnetization curves obtained with the magnetic field sequentially parallel to the cube axes. Brecher (1976b).

Table 14: 300° K hysteresis loop parameters for cubes 73215,21 and ,34. Brecher (1976b).

		J_s (e.m.u./g)	Fe° (wt.%)	$\langle J_{rs} \rangle$ (e.m.u./g) $\times 10^{-2}$	$\frac{\langle J_{rs} \rangle}{J_s}$	$\chi_p \left(\frac{\text{e.m.u.}}{\text{Oe g}}\right) \times 10^{-6}$	Fe^{++} (wt.%)	$\frac{Fe^{\circ}}{Fe^{++}}$	H_c (Oe)	$\chi_0 \times 10^{-4}$	J_s/χ_0
H‖NS	21	.263	.1195	.148	.0056	12	5.58	.0215	14	.85	3100
	34	.3095	.14	.151	.0049	14	6.59	.021	10	.925	3350
H‖EW	21	.267	.121	.0684	.0025	13.95	6.49	.0186	10	.8–.83	3300
	34	.338	.153	.177	.0052	13.18	6.13	.025	3	.966	3500
H‖TB	21	.271	.123	.12	.0044	14.7	6.87	.018	10	1	2700
	34	.346	.157	.2	.0058	13.6	6.33	.0247	38	1.2	2900